Observational and computational studies of atmospheric particle formation

Thesis by
Ryan Xavier Ward

In Partial Fulfillment of the Requirements for the
Degree of
Doctor of Philosophy

Caltech

CALIFORNIA INSTITUTE OF TECHNOLOGY
Pasadena, California

2025
Defended July 22, 2024

ACKNOWLEDGEMENTS

colleagues for life. Reina, Elyse, Sophia, Stephanie, Stavros, Kat, Chris, Yuanlong, Mingyi, Buddhi, and many others are owed many, many drinks on my dime.

Prof. Chang-Yu Wu was my first research advisor, and to this day I have not met a scientist whom I wish I could be more like. He is the combination of brilliant, humble, and hilarious to which I will always strive.

The friends I met in graduate school have become some of my best. My roommates from the Treatment Sanctuary[1] gave me incredible memories; grad school would have been immeasurably worse without you. To Costa I owe particular thanks; he was there for the highest highs and lowest lows, and offered me extreme patience in teaching me the basics of coding and atmospheric physics. I have so many other friends from all walks of life. I'm not corny enough to keep going, but I thank you all immensely.

Being a staff member[2] at the Chino Hills High School Drumline was my most cherished project in grad school. I assuredly traded research progress, papers, and time to spend hours at rehearsals and competitions, and in hindsight I only wish I started sooner. Having the structure of teaching to counter the nebulous and unstructured job of graduate research was something I didn't know I needed until I realized it was ending. To the students and staff, I am exceedingly grateful for our time spent together. Thank you to Ian for bringing me in, I owe you immeasurably. I also have to give a shout out to my high school percussion teacher Samantha J. Cope; she encouraged me to pursue this avenue, and she showed me in high school, and later in college, that you could simultaneously be a compassionate educator, an incredible musician, a prolific scientist, and an amazing person. To this day she is one of my biggest role models.

My parents have never questioned my professional decisions, although the discerning eye among them most certainly did. Thank you for always believing in and supporting me.

---

[1] A house turned rehab center turned house in San Marino which we acquired during the pandemic.

[2] For legal reasons, and in the eyes of Caltech, this is a volunteer position which did not impact my research hours.

ABSTRACT

Aerosols are a ubiquitous component of the atmosphere, playing pivotal roles in air quality and climate. This thesis explores the way these particles come to be, and their roles in these atmospheric processes.

Aerosols form from a variety of anthropogenic and biogenic activities, processes which are very prominent in urban settings. In Los Angeles, the last decade of research has been dominated by the role of summertime secondary organic aerosol (SOA) in contributing to particulate matter (PM). Here, we make observations in the equinox seasons and in the winter and detail the formation of atmospheric aerosols in these seasons. Using aerosol mass spectrometry, we demonstrate that ammonium nitrate persists as one of the dominant secondary aerosol components despite dramatic reductions in nitrogen oxide (NO_x) emissions. Further, we show that this ammonium nitrate is not measured by routine air quality measurements, biasing regulatory $PM_{2.5}$ measurements. In the wintertime, similar techniques demonstrate that primary organic aerosol, as opposed to secondary, is an important component of the $PM_{2.5}$, contrary to the prevailing narratives that SOA dominates the aerosol mass.

At global scales, the role of these aerosols in cloud formation and climate processes is of primary interest. While a variety of physicochemical properties of aerosols are important in the formation of cloud droplets, we focus here on the specific process of organic surface-partitioning. It has been suggested that in phase-separated aerosol, organic-rich surface layers can depress the surface tension of the particles, lowering their barrier to activate into cloud droplets. We assess this propensity for surface tension depression in two SOA systems, α-pinene and β-caryophyllene. Synergizing laboratory measurements, a thermodynamic model, and field data, it is shown that surface-active organics in these SOA systems can impact their hygroscopicity, though perhaps not sufficiently to warrant inclusion of these processes in global-scale models.

PUBLISHED CONTENT AND CONTRIBUTIONS

Chea, P. H., Pushpawela, B., Ward, R. X., & Flagan, R. C. (2024). Is double masking even worthwhile? *Aerosol Science and Technology*, 1–13. https://doi.org/10.1080/02786826.2024.2369638
RXW prepared experimental equipment and reviewed/edited the manuscript.

Pennington, E. A., Wang, Y., Schulze, B. C., Seltzer, K. M., Yang, J., Zhao, B., Jiang, Z., Shi, H., Venecek, M., Chau, D., Murphy, B. N., Kenseth, C. M., Ward, R. X., Pye, H. O. T., & Seinfeld, J. H. (2024). An updated modeling framework to simulate Los Angeles air quality – Part 1: Model development, evaluation, and source apportionment. *Atmospheric Chemistry and Physics*, *24*(4), 2345–2363. https://doi.org/10.5194/acp-24-2345-2024
RXW collected data and reviewed/edited the manuscript.

Pfannerstill, E. Y., Arata, C., Zhu, Q., Schulze, B. C., Ward, R., Woods, R., Harkins, C., Schwantes, R. H., Seinfeld, J. H., Bucholtz, A., Cohen, R. C., & Goldstein, A. H. (2024). Temperature-dependent emissions dominate aerosol and ozone formation in Los Angeles. *Science*, *384*(6702), 1324–1329. https://doi.org/10.1126/science.adg8204
RXW collected data and reviewed/edited the manuscript.

Schulze, B. C., Kenseth, C. M., Ward, R. X., Pennington, E. A., Rooy, P. V., Tasnia, A., Barletta, B., Meinardi, S., Morris, M., Jensen, A., Huang, Y., Parker, H. A., Hasheminassab, S., Day, D., Campuzano-Jost, P., de Gouw, J., Jimenez, J. L., Barsanti, K. C., Pye, H. O. T., . . . Seinfeld, J. H. (2024). Insights into the complex effects of reduced mobile source emissions on. *To Be Submitted*.
RXW collected data and reviewed/edited the manuscript.

De Jong, E. K., Singer, C. E., Azimi, S., Bartman, P., Bulenok, O., Derlatka, K., Dula, I., Jaruga, A., Mackay, J. B., Ward, R. X., & Arabas, S. (2023). New developments in PySDM and PySDM-examples v2:collisional breakup, immersion freezing, dry aerosol initialization, andadaptive time-stepping. *Journal of Open Source Software*, *8*(84), 4968. https://doi.org/10.21105/joss.04968
RXW contributed to development of surface-active organics code.

Nussbaumer, C. M., Place, B. K., Zhu, Q., Pfannerstill, E. Y., Wooldridge, P., Schulze, B. C., Arata, C., Ward, R., Bucholtz, A., Seinfeld, J. H., Goldstein, A. H., & Cohen, R. C. (2023). Measurement report: Airborne measurements of NO_x fluxes over Los Angeles during the RECAP-CA 2021 campaign. *Atmospheric Chemistry and Physics*, *23*(20), 13015–13028. https://doi.org/10.5194/acp-23-13015-2023
RXW collected data and reviewed/edited the manuscript.

Pushpawela, B., Chea, P., Ward, R., & Flagan, R. C. (2023). Quantification of face seal leakage using parallel resistance model. *Physics of Fluids*, *35*(12), 127127. https://doi.org/10.1063/5.0177717
RXW prepared experimental equipment and reviewed/edited the manuscript.

Schulze, B. C., Ward, R. X., Pfannerstill, E. Y., Zhu, Q., Arata, C., Place, B., Nussbaumer, C., Wooldridge, P., Woods, R., Bucholtz, A., Cohen, R. C., Goldstein, A. H., Wennberg, P. O., & Seinfeld, J. H. (2023). Methane Emissions from Dairy Operations in California's San Joaquin Valley Evaluated Using Airborne Flux Measurements. *Environmental Science & Technology*, *57*(48), 19519–19531. https://doi.org/10.1021/acs.est.3c03940
RXW collected data and reviewed/edited the manuscript.

Amanatidis, S., Huang, Y., Pushpawela, B., Schulze, B. C., Kenseth, C. M., Ward, R. X., Seinfeld, J. H., Hering, S. V., & Flagan, R. C. (2021). Efficacy of a portable, moderate-resolution, fast-scanning differential mobility analyzer for ambient aerosol size distribution measurements. *Atmospheric Measurement Techniques*, *14*(6), 4507–4516. https://doi.org/10.5194/amt-14-4507-2021
RXW collected data and reviewed/edited the manuscript.

Ming, Y., Loeb, N. G., Lin, P., Shen, Z., Naik, V., Singer, C. E., Ward, R. X., Paulot, F., Zhang, Z., Bellouin, N., Horowitz, L. W., Ginoux, P. A., & Ramaswamy, V. (2020). Assessing the influence of COVID-19 on the shortwave radiative fluxes over the East Asian Marginal Seas. *Geophysical Research Letters*. https://doi.org/10.1029/2020gl091699
RXW prepared and analyzed MODIS data and reviewed/edited the manuscript.

TABLE OF CONTENTS

LIST OF ILLUSTRATIONS

LIST OF TABLES

Chapter 1

INTRODUCTION

When discussing atmospheric aerosols, we are often explicitly concerned with the solid and liquid phases of the atmosphere, despite the formal definition of the word to include the gas-phase in which these particles are suspended. It is not that we are unconcerned with the gas phase, but to include this phase now concerns the entirety of the atmosphere, and the scope of the liquid and solid phases provides ample opportunity for research already. Implicitly, we will concern ourselves with this gas to the extent that it impacts the formation of the aerosols.

Semantics aside, it is not difficult to justify the study of atmospheric aerosols. These particles play an important role in the radiative budget of the planet, both directly, as scatterers of incident solar radiation [and outgoing terrestrial radiation], and indirectly, as the seeds upon which clouds form (cloud condensation nuclei, CCN) (Seinfeld & Pandis, 2016). Air pollution, within which particulate matter is a primary component, is one of the leading contributors to global mortality (Burnett et al., 2018; Cohen et al., 2017). Further, an understanding of aerosol physics and chemistry is important in a variety of contexts, such as the transmission of respiratory diseases (Lednicky et al., 2020) or the occupational risks associated with the production of fumes in combustion processes (Biswas & Wu, 2005). This thesis will explore aerosols in both the air quality and climate contexts through a variety of techniques, both experimental and computational.

1.1 Climate

As alluded to, it has been known for decades that atmospheric aerosols play an important role in climate by serving both as scatterers of solar radiation and as the nuclei upon which clouds form (Seinfeld & Pandis, 2016; Twomey, 1974), shown graphically in Figure 1.1. In the latest report from the Intergovernmnetal Panel on Climate Change (IPCC), it is estimated that the sum of the direct and indirect effects exert a radiative impact that masks up to half of the radiative impacts of CO_2 (Intergovernmental Panel On Climate Change, 2023). However, this estimate is not without uncertainty. It is often a parroted misnomer in the field that "aerosols represent the highest uncertainty in climate"; this is not true. The climate system is complex; the turbulence of the flows in the atmosphere are inherently stochastic,

imparting deep uncertainty to future predictions of climate. Further still, our understanding of the geopolitical events which will underpin the human response to climate are unpredictable. What is true is that compared to other radiative forcers (e.g., greenhouse gases), the uncertainty relative to the magnitude of the aerosol radiative forcing is one of the highest, in no small part because of our lack of knowledge of the preindustrial atmospheric aerosol burden. Even the sign of the aerosol forcing remains contentious (Bellouin et al., 2020).
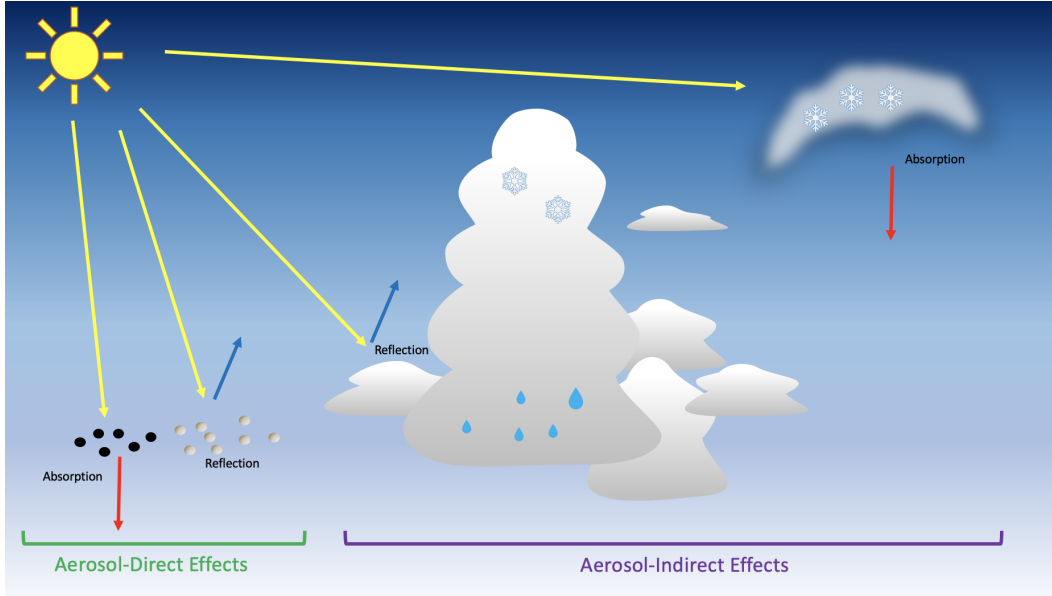
Figure 1.1: Cartoon of Earth's radiative budget with respect to aerosols.

In this thesis, we are most concerned with the indirect effects of aerosols; that is the impacts that aerosols exert on the climate system via clouds. The uncertainty associated with the indirect effect is multifaceted: the size and availability of aerosols, water vapor, and various energy fluxes all respond to perturbations both internal and external to the cloud in highly nonlinear ways (Ghan et al., 2016; Seinfeld et al., 2016). It is easiest to think about a simple chain rule in trying to tease out these interactions; for instance this forcing may adjust to aerosols in the following way:

$$F_{aci} = F_s \frac{\partial \alpha}{\partial \ln N_d} \frac{\partial \ln N_d}{\partial \ln N_{ccn}} \Delta \ln N_{ccn} \tag{1.1}$$

where we have related the radiative forcing of aerosol-cloud interactions (F_{aci}) to the downward solar radiative flux density (irradiance) above clouds (F_s), the cloud albedo (α), the cloud droplet number concentration (N_d), and a CCN descriptor (N_{ccn}) (Quaas et al., 2020). Of course, we can ask what modulates CCN concentra-

tions, and for instance expand this chain:

$$F_{aci} = F_s \frac{\partial \alpha}{\partial \ln N_d} \frac{\partial \ln N_d}{\partial \ln N_{ccn}} \frac{\partial \ln N_{ccn}}{\partial \ln E_{ccn}} \frac{\partial \ln E_{ccn}}{\partial \ln T} \Delta \ln T \qquad (1.2)$$

where now we have modulated the CCN concentration by a temperature-dependent (T) emission rate (E_{ccn}). Of course, aerosols feedback onto temperature, and therefore emissions, and so it becomes apparent that this system is inherently complex, and begs this question: what is the level of complexity needed for a model to accurately represent the global aerosol-indirect effects?

One useful model for assessing the impacts of aerosols on clouds is the so-called κ-Köhler model; κ is a catch-all descriptor of the aerosol which relates the physico-chemical properties and size to its propensity for water-uptake (Petters & Kreiden-weis, 2007). Many assumptions are baked into this model, particularly one that the activation of aerosols into cloud droplets proceeds with a surface tension equivalent to water. However, recent work has suggested that organics on the surface of aerosols may depress the surface tension (Davies et al., 2018; Lowe et al., 2019), thereby increasing their CCN activity (add another term to Equation 1.2). A tension arises: the simplicity of the κ framework is useful in a modeling context in saving the computational complexity of describing aerosol properties; at the same time, we are trading off physically realistic descriptions of the aerosol. Yet, this framework in its simplest form is still too complex for understanding aerosol-cloud interactions at a global scale, and so we must acknowledge these trade-offs at the limits of our current computational capacities.

1.2 Air Quality

Beyond their impacts on climate, the other primary focus of this thesis is the role of atmospheric aerosols in air pollution, particularly in the Los Angeles Basin. The first documented case of severe smog in the city is 1943, with visibility reported at only 3 blocks (CARB, 2023); the fact that the problem persists today is evidence of its complexity. However, the basics of this problem have also long been acknowledged; indeed, the meteorology, basin topology, and atmospheric chemistry all drive the intense aerosol formation (Haagen-Smit, 1952; Magill, 1949). Landmark legislation, like the federal Clean Air Act, and stringent local regulations (from the California Air Resources Board and the South Coast Air Quality Management District) have decreased all air pollutants significantly over the last decade (CARB, 2023), though Los Angeles County remains a non-attainment area for PM$_{2.5}$ (EPA, 2024). This

non-attainment remains evident even in the foothills of Pasadena, the contrast shown in a couple photos I took not too far from Caltech's campus (Figure 1.2).

Figure 1.2: Images stitched together from Pasadena, CA on good and poor visibility days.

While we have made strides in reducing the most easily understood reactants of the air quality problem (e.g., NO_x), the scale and breadth of the emissions and transformation we need to understand are vast. In addition to traditional sources, like those of vehicular and biogenic origin, we are now concerned with those from nontraditional sources, such as those from volatile chemical products or asphalt (Khare et al., 2020; McDonald et al., 2018). How these precursors respond to oxidant levels and temperature additionally influences their SOA formation potential in highly nonlinear ways (Nussbaumer & Cohen, 2021; Pennington et al., 2021; Pfannerstill et al., 2024; Seltzer et al., 2021). Much in the same vain of the aerosol climate question, we are at a crossroads between detailed, process-level descriptions of the chemistry against the computational cost to constrain the problem (Pennington et al., 2023).

1.3   Organization of Thesis

Chapters two and three of this thesis deal with the impacts of aerosols on air quality. While summer has been the most heavily investigated and colloquially discussed season in terms of urban atmospheric chemistry, we focus on the equinox seasons and winter. In Chapter 2, we revisit one of LA's most prominent air pollutants,

ammonium nitrate, discussing how its formation has changed over decades, and how it persists as a major problem for LA air regulators. In Chapter 3, we discuss winter air quality in LA; similar to ammonium nitrate, we make measurements that seem reminiscent of 20th century air quality issues, discussing the role of primary organics as a dominant contributor to poor air quality.

In Chapter 4, the focus shifts to the climate impacts of aerosols. Here, we explore the role that organic aerosol can play in the activation of cloud droplets through its modification of surface tension, and we apply laboratory results to real world data to try and chip away at the necessary level of chemical complexity required of cloud-resolving models to accurately reflect the atmospheric aerosol.

In the appendices, I have included a number of contributions for which I am not the lead author but contributed to over the course of my PhD. Indeed, if you sampled my work time at random throughout graduate school, you would more often than not find me engaged in some campaign in which I was not often the primary scientist; this is the nature of our work, contributing our skills where the scientific questions and the policy problems arise. The common thread of aerosols weaves in and out of all of these papaers. It was not something I expected when I started working in the field, but knowledge of fundamental aerosol science and engineering equips you with a skillset to work in a variety of applied topics. While atmospheric chemistry and physics has been my primary application of aerosol science in this thesis, topics ranging airborne disease transmission and instrument design are touched in these papers. It has been an unintentional and very pleasant surprise to be able to work on such a breadth of subject matter.

References

Bellouin, N., Quaas, J., Gryspeerdt, E., Kinne, S., Stier, P., Watson-Parris, D., Boucher, O., Carslaw, K. S., Christensen, M., Daniau, A. L., Dufresne, J. L., Feingold, G., Fiedler, S., Forster, P., Gettelman, A., Haywood, J. M., Lohmann, U., Malavelle, F., Mauritsen, T., ... Stevens, B. (2020). Bounding Global Aerosol Radiative Forcing of Climate Change. *Reviews of Geophysics*, *58*(1), 1–45. https://doi.org/10.1029/2019RG000660

Biswas, P., & Wu, C.-Y. (2005). Nanoparticles and the Environment. *Journal of the Air & Waste Management Association*, *55*(July 2005), 708–746. https://doi.org/10.1080/10473289.2005.10464656

Burnett, R., Chen, H., Szyszkowicz, M., Fann, N., Hubbell, B., Pope, C. A., Apte, J. S., Brauer, M., Cohen, A., Weichenthal, S., Coggins, J., Di, Q., Brunekreef, B., Frostad, J., Lim, S. S., Kan, H., Walker, K. D., Thurston, G. D., Hayes,

R. B., . . . Spadaro, J. V. (2018). Global estimates of mortality associated with long-term exposure to outdoor fine particulate matter. *Proceedings of the National Academy of Sciences, 115*(38), 9592–9597. https://doi.org/10.1073/pnas.1803222115

CARB. (2023). California Air Resources Board History. Retrieved October 31, 2023, from https://ww2.arb.ca.gov/about/history

Cohen, A. J., Brauer, M., Burnett, R., Anderson, H. R., Frostad, J., Estep, K., Balakrishnan, K., Brunekreef, B., Dandona, L., Dandona, R., Feigin, V., Freedman, G., Hubbell, B., Jobling, A., Kan, H., Knibbs, L., Liu, Y., Martin, R., Morawska, L., . . . Forouzanfar, M. H. (2017). Estimates and 25-year trends of the global burden of disease attributable to ambient air pollution: An analysis of data from the Global Burden of Diseases Study 2015. *The Lancet, 389*(10082), 1907–1918. https://doi.org/10.1016/S0140-6736(17)30505-6

Davies, J. F., Zuend, A., & Wilson, K. R. (2018). Technical Note: The Role of Evolving Surface Tension in the Formation of Cloud Droplets. *Atmospheric Chemistry and Physics Discussions*, 1–30. https://doi.org/10.5194/acp-2018-1201

EPA. (2024). $PM_{2.5}$ (2012) Designated Area/State Information. Retrieved June 20, 2024, from https://www3.epa.gov/airquality/greenbook/kbtc.html

Ghan, S., Wang, M., Zhang, S., Ferrachat, S., Gettelman, A., Griesfeller, J., Kipling, Z., Lohmann, U., Morrison, H., Neubauer, D., Partridge, D. G., Stier, P., Takemura, T., Wang, H., & Zhang, K. (2016). Challenges in constraining anthropogenic aerosol effects on cloud radiative forcing using present-day spatiotemporal variability. *Proceedings of the National Academy of Sciences, 113*(21), 5804–5811. https://doi.org/10.1073/pnas.1514036113

Haagen-Smit, A. J. (1952). Chemistry and Physiology of Los Angeles Smog. *Industrial & Engineering Chemistry, 44*(6), 1342–1346. https://doi.org/10.1021/ie50510a045

Intergovernmental Panel On Climate Change. (2023, July). *Climate Change 2021 – The Physical Science Basis: Working Group I Contribution to the Sixth Assessment Report of the Intergovernmental Panel on Climate Change* (1st ed.). Cambridge University Press. https://doi.org/10.1017/9781009157896

Khare, P., Machesky, J., Soto, R., He, M., Presto, A. A., & Gentner, D. R. (2020). Asphalt-related emissions are a major missing nontraditional source of secondary organic aerosol precursors. *Science Advances, 6*(36), eabb9785. https://doi.org/10.1126/sciadv.abb9785

Lednicky, J. A., Lauzardo, M., Fan, Z. H., Jutla, A., Tilly, T. B., Gangwar, M., Usmani, M., Shankar, S. N., Mohamed, K., Eiguren-Fernandez, A., Stephenson, C. J., Alam, M. M., Elbadry, M. A., Loeb, J. C., Subramaniam, K., Waltzek, T. B., Cherabuddi, K., Morris, J. G., & Wu, C.-Y. (2020). Viable SARS-CoV-2 in the air of a hospital room with COVID-19 patients. *International*

Journal of Infectious Diseases, *100*, 476–482. https://doi.org/10.1016/j.ijid.2020.09.025

Lowe, S. J., Partridge, D. G., Davies, J. F., Wilson, K. R., Topping, D., & Riipinen, I. (2019). Key drivers of cloud response to surface-active organics [Publisher: Springer US]. *Nature Communications*, *10*(1). https://doi.org/10.1038/s41467-019-12982-0

Magill, P. L. (1949). The Los Angeles Smog Problem. *Industrial & Engineering Chemistry*, *41*(11), 2476–2486. https://doi.org/10.1021/ie50479a027

McDonald, B. C., De Gouw, J. A., Gilman, J. B., Jathar, S. H., Akherati, A., Cappa, C. D., Jimenez, J. L., Lee-Taylor, J., Hayes, P. L., McKeen, S. A., Cui, Y. Y., Kim, S. W., Gentner, D. R., Isaacman-VanWertz, G., Goldstein, A. H., Harley, R. A., Frost, G. J., Roberts, J. M., Ryerson, T. B., & Trainer, M. (2018). Volatile chemical products emerging as largest petrochemical source of urban organic emissions. *Science*, *359*(6377), 760–764. https://doi.org/10.1126/science.aaq0524

Nussbaumer, C. M., & Cohen, R. C. (2021). Impact of OA on the Temperature Dependence of $PM_{2.5}$ in the Los Angeles Basin. *Environmental Science & Technology*, *55*(6), 3549–3558. https://doi.org/10.1021/acs.est.0c07144

Pennington, E. A., Seltzer, K. M., Murphy, B. N., Qin, M., Seinfeld, J. H., & Pye, H. O. T. (2021). Modeling secondary organic aerosol formation from volatile chemical products [Publisher: Copernicus GmbH]. *Atmospheric Chemistry and Physics*, *21*(24), 18247–18261. https://doi.org/10.5194/acp-21-18247-2021

Pennington, E. A., Wang, Y., Schulze, B. C., Seltzer, K. M., Yang, J., Zhao, B., Jiang, Z., Shi, H., Venecek, M., Chau, D., Murphy, B. N., Kenseth, C. M., Ward, R. X., Pye, H. O. T., & Seinfeld, J. H. (2023). An Updated Modeling Framework to Simulate Los Angeles Air Quality. Part 1: Model Development, Evaluation, and Source Apportionment [Publisher: Copernicus GmbH]. *EGUsphere*, 1–27. https://doi.org/10.5194/egusphere-2023-749

Petters, M. D., & Kreidenweis, S. M. (2007). A single parameter representation of hygroscopic growth and cloud condensation nucleus activity. *Atmospheric Chemistry and Physics*, *13*(2), 1961–1971. https://doi.org/10.5194/acp-13-1081-2013

Pfannerstill, E. Y., Arata, C., Zhu, Q., Schulze, B. C., Ward, R., Woods, R., Harkins, C., Schwantes, R. H., Seinfeld, J. H., Bucholtz, A., Cohen, R. C., & Goldstein, A. H. (2024). Temperature-dependent emissions dominate aerosol and ozone formation in Los Angeles. *Science*, *384*(6702), 1324–1329. https://doi.org/10.1126/science.adg8204

Quaas, J., Arola, A., Cairns, B., Christensen, M., Deneke, H., Ekman, A., Feingold, G., Fridlind, A., Gryspeerdt, E., Hasekamp, O., Li, Z., Lipponen, A., Ma, P.-L., Mülmenstädt, J., Nenes, A., Penner, J., Rosenfeld, D., Schrödner, R.,

Sinclair, K., . . . Wendisch, M. (2020). Constraining the Twomey effect from satellite observations: Issues and perspectives. *Atmospheric Chemistry and Physics Discussions*, (May), 1–31. https://doi.org/10.5194/acp-2020-279

Seinfeld, J. H., & Pandis, S. N. (2016). *Atmospheric Chemistry and Physics: From Air Pollution to Climate Change*. Wiley & Sons.

Seinfeld, J. H., Bretherton, C., Carslaw, K. S., Coe, H., Demott, P. J., Dunlea, E. J., Feingold, G., Ghan, S., Guenther, A. B., Kahn, R., Kraucunas, I., Kreidenweis, S. M., Molina, M. J., Nenes, A., Penner, J. E., Prather, K. A., Ramanathan, V., Ramaswamy, V., Rasch, P. J., . . . Wood, R. (2016). Improving our fundamental understanding of the role of aerosol cloud interactions in the climate system. *Proceedings of the National Academy of Sciences of the United States of America*, *113*(21), 5781–5790. https://doi.org/10.1073/pnas.1514043113

Seltzer, K. M., Pennington, E., Rao, V., Murphy, B. N., Strum, M., Isaacs, K. K., & Pye, H. O. T. (2021). Reactive organic carbon emissions from volatile chemical products. *Atmospheric Chemistry and Physics*, *21*(6), 5079–5100. https://doi.org/10.5194/acp-21-5079-2021

Twomey, S. (1974). Pollution and the planetary albedo. *Atmospheric Environment (1967)*, *8*(12), 1251–1256. https://doi.org/https://doi.org/10.1016/0004-6981(74)90004-3

Chapter 2

THE PERSISTENCE AND PATHOLOGIES OF AMMONIUM NITRATE SMOG IN LOS ANGELES

Ryan X. Ward, Haroula D. Baliaka, Benjamin C. Schulze, Gaige H. Kerr, Sina Hasheminassab, John D. Crounse, Roya Bahreni, Ann M. Dillner, Armistead Russell, Nga L. Ng, Paul O. Wennberg, Richard C. Flagan, and John H. Seinfeld

[Intentionally redacted.]

Chapter 3

PRIMARY ORGANIC AEROSOL IMPORTANT TO UNDERSTANDING POOR WINTERTIME AIR QUALITY IN LOS ANGELES

Ryan X. Ward, Haroula D. Baliaka, Benjamin C. Schulze, Sina Hasheminassab, Paul O. Wennberg, Richard C. Flagan, and John H. Seinfeld

3.1 Abstract

The Los Angeles basin is well known for its historically poor air quality and, despite strengthening of regulations, declines in particulate matter (PM) concentrations have stagnated over the last decade. Comprehensive, multi-institutional surveys of air quality in Los Angeles (e.g., CalNex) have been most frequently performed in the summer (nominally when routine air quality measurements of PM are highest) and have revealed that much of the aerosol pollution is driven by oxygenated secondary organic aerosol (SOA). In this work, we deploy a suite of aerosol- and gas-phase instruments to characterize the wintertime atmosphere between January and March in Pasadena, CA, including a ToF-ACSM with $PM_{2.5}$ inlet for aerosol composition. We observe PM loadings that are often comparable to summertime AMS measurements of organic aerosol, but with a diurnal cycle whose maximum appears in the evening as opposed to the afternoon. Positive matrix factorization of the mass spectral data shows that, in contrast to the summer, the aerosol is majority primary in nature (as opposed to secondary). Further, we compare with routine air quality measurements of PM, CO, and NO_x, which largely suggests that boundary layer dynamics play a dominant role in the shifted diurnal profile, and additionally that this profile is a robust feature of the wintertime atmosphere in Los Angeles. These results imply that acknowledgment of primary emitters of particulate matter, such as mobile or cooking sources, is still critical for understanding the aerosol composition and reducing air pollution in the Los Angeles basin.

3.2 Introduction

In many urban locations across the world, organic aerosol (OA) composes a majority of the submicron Particulate Matter (PM). Evidence from aerosol mass spectrometry, specifically measurements by the Aerodyne aerosol mass spectrometer (AMS),

suggests this OA is largely secondary in origin, meaning it is produced from chemical reactions in the atmosphere (SOA), as opposed to primary, meaning it would be directly emitted (POA) (Jimenez et al., 2009; Zhang et al., 2007). Worth noting, this delineation between POA and SOA is not so rigid; POA can contain semi-volatile species which, at atmospheric conditions, may evaporate after emission, undergo oxidative chemistry, and re-condense to the particle phase (Robinson et al., 2007; Shrivastava et al., 2006). Semantics aside, having these classifications is important from a regulatory perspective, as the links between POA and their emission sources are much clearer than for SOA (Kleeman & Cass, 2001; Seinfeld & Pandis, 2016). Further, it is likely that toxicity of the PM components are different, some studies linking the primary component with a higher intrinsic toxicity (Tuet et al., 2017; Verma et al., 2015), though long-term negative health impacts can likely be ascribed to all PM components (Wang et al., 2022; Wyzga & Rohr, 2015).

The Los Angeles basin is no exception to this rule, plagued by some of the highest OA concentrations in the country and often exceeding the EPA's National Ambient Air Quality Standards for PM (EPA, 2024). The prevailing narrative around Los Angeles air quality, like many cities around the world, is that secondary organic aerosol (SOA) constitutes the majority of the total OA (Hayes et al., 2013; Hersey et al., 2011; Schulze et al., 2024). While this is not without evidence, it is interesting to note that in arguably the most seminal urban OA characterization paper, only 3 of the 24 campaigns report winter measurements (Jimenez et al., 2009). Specifically in Los Angeles, the major contemporary field campaigns using aerosol mass spectrometry (e.g., CalNex, RECAP, or CalNexT) to characterize the aerosol have all occurred in the summer, possibly generating a summertime bias to our understanding of Los Angeles OA. Studies predating aerosol mass spectrometry (circa 1980s/90s) demonstrated that the majority of fine particle organic mass was associated with primary emission sources (Kleeman & Cass, 2001; Schauer et al., 1996). It is worth acknowledging that as we define it now, some fraction of this "primary OA" could evaporate to form SOA, and so again we must accept that our definitions of POA/SOA are elastic. Today, a 1:1 mapping of what we source apportion by mass spectrometry to what we call SOA and POA in bottom-up model studies is not always possible (Ma et al., 2017).

Studies shave shown that temperature-dependent emissions dominate the secondary aerosol in LA (Nussbaumer & Cohen, 2021; Pfannerstill et al., 2024), which would suggest that summertime is indeed the greatest concern for large OA concentrations.

However, emissions less sensitive to temperature, like mobile sources and volatile chemical products (VCPs) have also been linked to contributing to the OA, principally the SOA (Jathar et al., 2017; McDonald et al., 2018; Zhao et al., 2022), which potentially contradicts this summertime OA narrative. However, this only accounts for the source of emissions; indeed the rate of aerosol production is a function of the oxidative condition of the urban air and other meteorological conditions, both which may favor or disfavor summertime OA production (Hass-Mitchell et al., 2024; Schulze et al., 2024). Observations from routine monitoring stations in Los Angeles suggest two important points: (1) the seasonally averaged $PM_{2.5}$ is roughly constant throughout the year; and (2) primary emissions, such as those from mobile sources, make up a larger fraction of the PM in the winter (Hasheminassab, Daher, Saffari, et al., 2014). Further, total carbon analyses suggest that while the SOA dominates in the summer, the POA is actually of similar order importance to the SOA, and the total OA magnitude is comparable across seasons (Ivančič et al., 2022).

In this work, we provide mass spectral measurements of the $PM_{2.5}$ in Los Angeles with an Aerosol Chemical Speciation Monitor (ACSM), a type of aerosol mass spectrometry (Fröhlich et al., 2013). We show that POA, and in particular the cooking-influenced POA, contribute more than half of the wintertime OA in 2023. Further, we demonstrate this is likely a robust feature of the Los Angeles basin, suggesting a seasonal regulatory strategy for the PM in controlling primary aerosol.

3.3 Methods

The Winter Air Quality Study (WAQS-LA) was run from January 26 to March 6, 2023, where air quality measurements were made from the roof of Caltech Hall (~40 m above ground level) in Pasadena, CA. The primary particle phase instruments deployed were an Aerodyne ToF-ACSM with $PM_{2.5}$ inlet (hereafter ACSM) and a TSI Scanning Mobility Particle Sizer (SMPS; Classifer Model 3082, water CPC Model 3789). The ACSM measures the non-refractory chemical composition of the aerosol (Fröhlich et al., 2013) and is a $PM_{2.5}$ equivalent size measurement. Non-refractory is an operational definition for the aerosol which vaporize at 600 °C, which is thought to represent a substantial portion of the aerosol mass in Los Angeles (one notable exception being black carbon, which is refractory) (Schulze et al., 2024). The SMPS infers the size distribution of the aerosol from electrical mobility measurements and is a PM_1 measurement. The sample was drawn at a total flow rate of 2 lpm through 7 m of 3/8" stainless steel line attached to a Teflon-coated cyclone (0.6 lpm for the SMPS, 0.1 for the ACSM, and 1.3 lpm in make-up flow).

The instrument ionization efficiency (IE) and realtive ioniization efficiencies (RIE) were calibrated with 300 nm ammonium nitrate and ammonium sulfate particles.

The ACSM analysis was performed with Tofware. For this data set, the composition dependent collection efficiencey is applied (Middlebrook et al., 2012), and the UMR elemental ratios (O:C and H:C) are estimated from the Improved-Ambient method (Canagaratna et al., 2015; Ng, Canagaratna, et al., 2011). Aerosol density is estimated according to the density of non-refractory component species, which neglects potential other PM components such as black carbon or metals (though we expect their contribution to the total mass to be low, see results). The organic aerosol density is inferred from the elemental ratios, and the inorganic components are lumped with a density of 1.75 g cm^{-3}(Hu et al., 2020; Kuwata et al., 2012). Positive Matrix Facotrization (PMF) analysis was performed on the OA data to aid in source identification. Briefly, PMF deconvolves the observed ambient spectra into components under the constraint of non-negativity, which creates physical component spectra which can be attributed to real-world sources (Paatero, 1997; Paatero & Tapper, 1994; Zhang et al., 2011). Detailed explanation of the 3-factor PMF optimal solution is presented in the Supporting Information.

Trace gas and meteorological measurements were made by the South Coast Air Quality management District (SCAQMD) at their Pasadena site, roughly 500 m from Caltech Hall. These measurements include: CO, NO_x, O_3, temperature, relative humidity, and wind speed/direction. Data are available through the Air Quality and Meteorological Information System (AQMIS). Temperature and relative humidity measurements were also made on Caltech's campus at the TCCON station, roughly 500 m from Caltech Hall.

The boundary layer height (BLH) data used in this study are from the ECMWF reanalysis product (Hersbach et al., 2023). Though we acknowledge there are issues when comparing mixing heights between reanalysis data and true measurements (Ware et al., 2016), the seasonal differences reported by the reanalysis data are consistent with measurements made in Southern California, particularly the relative heights and phasing of the shallowing of the BLH (Rahn & Mitchell, 2016). We are concerned here with employing the BLH as a tool to aid in discrimination of PMF factors and understanding the OA dynamics, as in previous work (L. Xu et al., 2015); so, its exact magnitude is not as pertinent as is necessary in studies quantifying, for instance, greenhouse gas fluxes (Schulze et al., 2023).

AMS measurments presented here are from Schulze et al. as part of the CalNexT

campaign, and so only a brief descriptions are provided here (Schulze et al., 2024). Measurements were performed at the same site (Caltech Hall) in the summer of 2022 from 7 July to 14 August. The principle difference between the summer and winter data arises in the mass spectral measurement; during CalNexT an Aerodyne HR-ToF-AMS (aerosol mass spectrometer) was used, which, among other differences, is a PM_1 measurement (DeCarlo et al., 2006; Jayne et al., 2000; Jimenez, 2003). The size range difference between the ACSM and the AMS lies primarily in the aerodynamic lens, designed in the ACSM for transmission of larger particles (W. Xu et al., 2017). PMF results from CalNexT are described thoroughly by Schulze et al., who identify a 4-factor solution for summertime LA compared to our 3-factor solution (we discuss these differences in the results).

3.4   Results and Discussion

Ambient Measurements and Source Apportionment

A summary diurnal profile of the WAQS-LA measurements is shown in Figure 3.1(a), contrasted with the summertime CalNexT measurements in 3.1(b). A full time series of the measurements is available in the Supplement (Figures 3.5 and 3.6). When comparing measurements in the winter and spring, we notice that the diurnal profiles are quite different. While the summertime peak in PM is during the afternoon, consistent with air masses arriving from downtown (Hayes et al., 2013), the wintertime peak is in the evening, likely as a result of a shallower evening boundary layer (see Supplement, Figures 3.7 and 3.8) (P. Sun et al., 2022). Further, the peaks of these diurnal profiles are of similar order, suggesting that wintertime PM is just as prominent as summertime (Hasheminassab, Daher, Saffari, et al., 2014). This is also apparent in the full time series data from each campaign, where it is clear that the PM maxima across the time series are of similar magnitude and frequency.

We observe higher nitrate concentrations in the winter than the summer, which we attribute to inorganic ammonium nitrate production, whose temperature-dependence favors colder wintertime temperatures (Pusede et al., 2016; Womack et al., 2019). We observe in the winter that a large fraction of the nitrate is associated with inorganic nitrate, as there are few departures from the ammonium balance (see Supplement, Figure 3.9) (Farmer et al., 2010). This contrasts the summertime data, where anywhere from 30 to 50% of the measured nitrate mass was associated with organic nitrates (Schulze et al., 2024). We observe lower sulfate concentrations (76% lower campaign average) in the winter than summer, which is consistent with
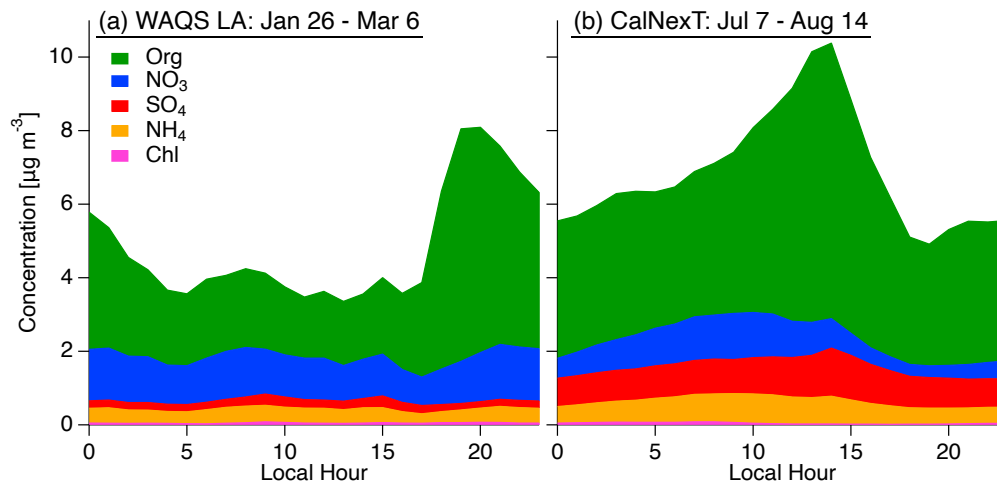
Figure 3.1: Diurnal profile for (a) wintertime Pasadena aerosol measurements by ACSM and (b) summertime Pasadena aerosol measurements by AMS.

our understanding of the photochemical production of sulfate in Los Angeles. For the inorganic components, these seasonalities agree with PMF on filter-based data in Los Angeles (Hasheminassab, Daher, Ostro, & Sioutas, 2014), and also with AMS observations in other urban locations such as Atlanta (L. Xu et al., 2015).

An important distinction between the summer and wintertime datasets lies in their measurement size cutoffs. Recall the winter measurement is a $PM_{2.5}$ measurement by the ACSM, while the summer measurement is a PM_1 measurement by the AMS. We can constrain the fraction of $PM_{2.5}$ mass in the PM_1 size range through the SMPS measurement; while the SMPS measures the total volume in the PM_1, we infer the mass through an estimation of the aerosol density (see Methods). For the WAQS-LA data, the ACSM and SMPS measurements roughly track each other (see Supplement, Figure 3.10), suggesting that the $PM_{2.5}$ is nominally PM_1. This is also true of the summertime data, although this need not be true in the LA Basin, as significant PM mass above 1 micron has been observed, for instance, when ammonium nitrate concentrations are high (Hughes et al., 2002). Also noteworthy is the y-intercept of the regression, landing at 0.85 μg m^{-3}; we attribute this to black carbon (BC), which is a refractory species not measured by the ACSM. 1 μg m^{-3} daily-average is as a rough order of magnitude expectation for BC concentrations in the LA basin (Ivančič et al., 2022).

For the wintertime dataset, we resolve a 3-factor solution for the OA from PMF, the diurnal profile shown in Figure 3.2(a). Additionally, we provide the UMR

spectra in the Supporting Information (Figure 3.11). We resolve two POA factors, a Hydrocarbon-like OA (HOA) and a Cooking-influenced OA (CIOA), and one SOA factor, which we have called Oxygenated OA (OOA). The two POA factors presented in this work are similar in source-type to those presented in previous AMS measurements in Los Angeles (Hayes et al., 2013; Schulze et al., 2024). The diurnal profile of the CIOA factor, when normalized for the height of the boundary layer (Figure 3.2(b)), is in good agreement between the two seasons and resolves two peaks (around lunchtime and dinnertime) which are of similar magnitude between seasons. Curiously, the CIOA factor resolved during CalNex (2010 LA) demonstrated two peaks, both later in the day, without needing this BLH normalization (Hayes et al., 2013). By comparison, the LA summertime CIOA factor exhibits a minimally pronounced lunchtime peak in 2024 compared to 2010. In other urban locations, the CIOA factor has also been observed with two peaks around meals (though at different times) (Crippa et al., 2013; Mohr et al., 2012; Y.-L. Sun et al., 2011; L. Xu et al., 2015).
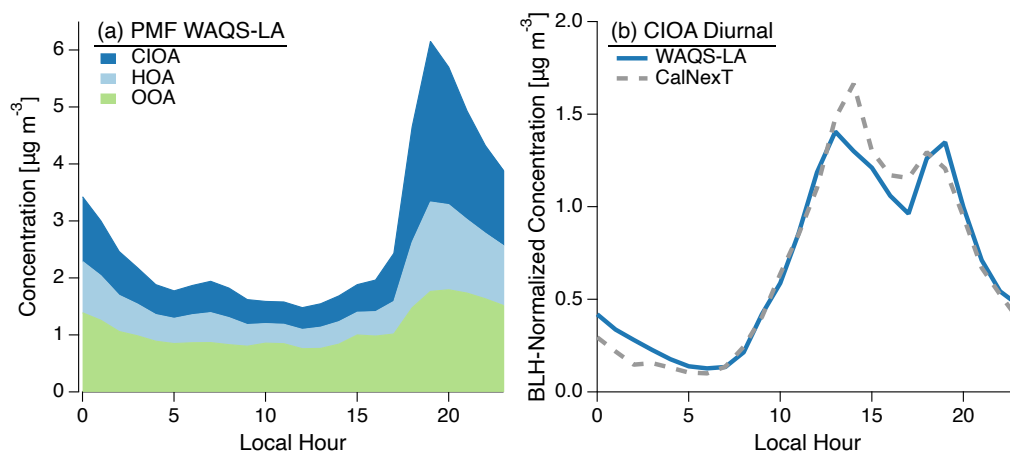
Figure 3.2: Diurnal profile for (a) the OA PMF solution and (b) the CIOA factor normalized to the boundary layer height for this work and for CalNexT.

Between winter and summer, the OOA, HOA, and CIOA spectra exhibit r^2 values of 0.88, 0.63, and 0.43, respectively. These are generally lower than spectra correlations between 2010 and 2024 AMS observations (minimum r^2 of 0.85), though both the instrument difference (AMS vs ACSM) and seasonality (winter vs summer) may play some role (Ng, Herndon, et al., 2011). In particular, changes in seasonality can impart quite large changes to the resolved factors, as been reported for the CIOA factor in Greece, possibly as a result of cooking type, or a result of different oxidative conditions of the volatile POA components (Kaltsonoudis et al., 2017).

The PMF results are summarized in Figure 3.3 for this work and other campaigns in Los Angeles utilizing aerosol mass spectrometry. It is evident that during the winter there is a large increase in the POA component of the aerosol, which in winter of 2023 was towards 57% of the measured $PM_{2.5}$. This wintertime enhancement has been reported by measurements of Total Carbon in Los Angeles, though is more subtle than reported here (Ivančič et al., 2022). It is important to note that it is the amount of POA relative to SOA that is enhanced between the seasons. We expect that the absolute magnitude of POA production/emission is tied to sources which lack as much seasonality as the photochemical drivers and thus production of SOA.
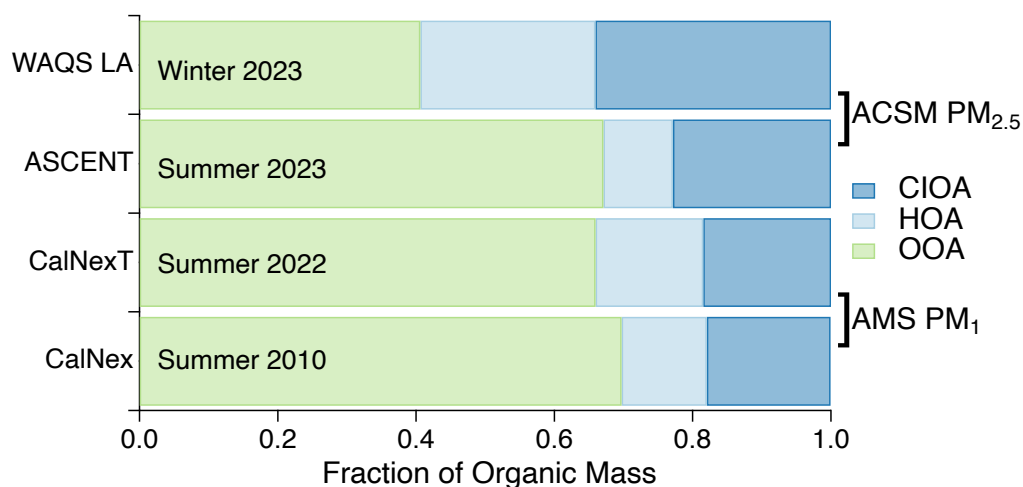
Figure 3.3: Comparison of AMS and ACSM measured PMF factors in Los Angeles in various seasons and campaigns. CalNex and CalNexT were measured by AMS in Pasadena, WAQS LA was measured by ACSM in Pasadena, and ASCENT was measured by ACSM in Pico Rivera (~10 mi south of Pasadena).

Regulatory Implications

To assess whether the data recorded here are representative of wintertime in Los Angeles, we performed a harmonic analysis of the diurnal cycle for a variety of locations, years, and seasons in the South Coast Air Quality Management District (SCAQMD; LA and Riverside Counties). This technique is quite common in the climate science literature (e.g., precipitation (Christopoulos & Schneider, 2021)) for understanding the diurnal cycle processes. Here, we fit seasonally-averaged, hourly measurements of $PM_{2.5}$ made by SCAQMD at four sites where hourly measurements are available: Downtown LA, Rivseride-Rubidoux, Glendora, and Burbank. These are hourly federal equivalence method data (e.g., by Beta Attenuation Monitor) available through AQMIS, and we use years in 2010 - 2023 and fit for winter (DJF)

and summer (JJA). We enforce the constraint that the PM diurnal cycle fit the first harmonic (that is there is only one maximum and one minimum in a 24 hr cycle), though we note that this is not necessarily true (e.g., rush hour traffic in the morning and evening provide peaks which do not track a purely sinusoidal diurnal cycle).

The data are fit to the following function:

$$C = A \sin (t + \phi) \tag{3.1}$$

where C is the measured concentration [μg m^{-3}], A is the amplitude of the diurnal cycle [μg m^{-3}], t is the hour of day (converted into radians), and ϕ is the phase. From this fit on the seasonally-average diurnal cycle, we extract two important parameters: the range of the diurnal cycle (A), and the timing of the PM maximum (calculated from ϕ). If a reasonable fit could not be achieved, we discard the fit (again, the data need not necessarily fit the first harmonic diurnal cycle).
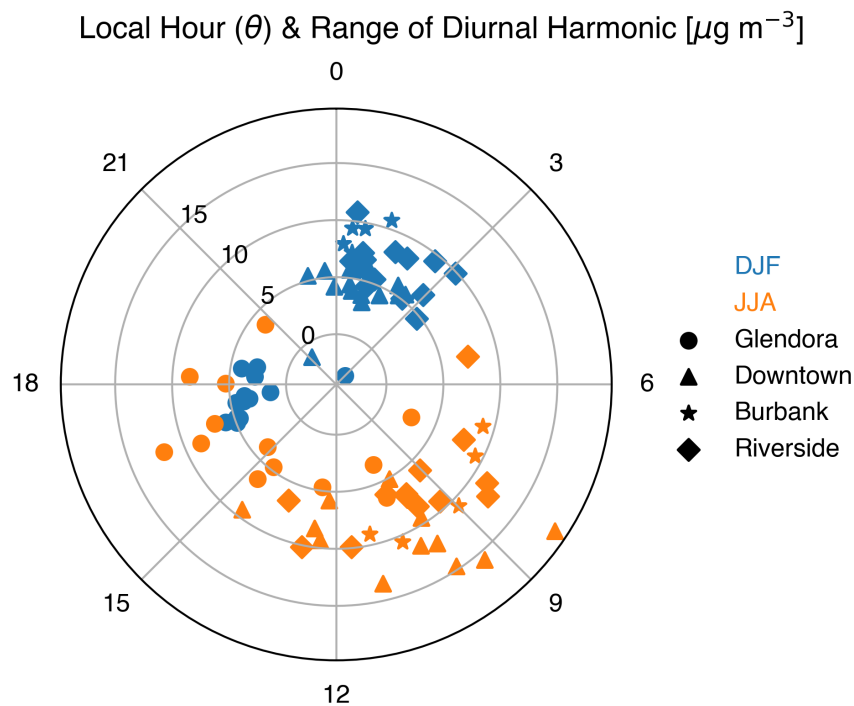
Figure 3.4: First harmonic of the diurnal cycle fit for various years, seasons, and locations in the South Coast Air Basin. The radial position represents the local hour and the radial position represents the amplitude of the diurnal cycle.

The results of the harmonic analysis are shown in Figure 3.4. The summertime data, those points in orange, suggest a variety of timings in the peak of aerosol loading

for the sites across the basin. This is consistent with both a a variety of chemical production terms in the summer in addition to our understanding of transport as a driver of daytime variability in Los Angeles air quality (Hayes et al., 2013; Warneke et al., 2013). We can draw two important conclusions for the wintertime data. First, the wintertime data cluster around a nighttime (post-sundown) maximum, which suggests the importance of meteorology and boundary layer dynamics in driving poor air quality. Physically, this is intuitive: for a shallower mixing height, the same emission profile will create a higher concentration. From our data, we can subsequently infer that primary emissions are important in driving high aerosol loadings. Second, the range in the diurnal cycle of PM is similar between summer and winter. This suggests that despite less photo-chemical activity and secondary aerosol production, wintertime aerosol dynamics are of similar concern from an air quality and human health perspective. In fact, it could be argued that because the organic aerosol component in the winter is denominated by POA, targeting its precursors is more straightforward than for summertime SOA. This work adds to the growing body of literature which suggests seasonality is an important parameter in regulatory action for reducing PM pollution (P. Sun et al., 2022).

3.5 Supporting Information

Ambient Measurements

A variety of ambient measurement supporting figures are presented here, including time series ACSM/AMS data, meteorological data, and other relevatn figures for the main text.

PMF Intepretation

Positive Matrix Factorization of the data was performed on the dataset, as in previous AMS studies (Hayes et al., 2013; Schulze et al., 2024; Zhang et al., 2011). A three and four factor solutions were resolved and interpretable, and we have opted for the 3-factor solution. These spectra are shown in Figures 3.11 and 3.12. In both solutions, HOA (hydrocarbon-like organic aerosol, commonly associated with vehicle combustion and chemically with longer-chain alkanes) and CIOA (cooking-inlfuenced OA) were resolved. However, between the three and four factor solution, one or two OOA factors were resolved, OOA in the 3-factor and LO-OOA and MO-OOA in the 4-factor. Between the 3 and 4-factor solutions, the difference in campaign averaged POA (sum of CIOA and HOA) is negligible (57% in the 3-factor and 56% in the 4-factor).

The 4-factor solution revolves similar factors to those reported in the summertime 2022 measurements. The r^2 values for the 4-factor spectra against their CalNexT counterparts are: 0.62 for HOA 0.62, 0.75 for CIOA, 0.40 for LO-OOA, and 0.91 for MO-OOA. Reprinted from the main text, the 3-factor OOA, HOA, and CIOA spectra exhibit r^2 values of 0.88, 0.63, and 0.43, respectively. The HOA has very similar r^2 between the 3- and 4-factor solutions. While the OOA and MO-OOA show good correlations (OOA is regressed to sum of LO+MO in the summer), the LO-OOA does not, possibly as a result of changing emission profiles of S/IVOCs between seasons. The CIOA factor exhibits worse correlation in the 3 than 4-factor solution, as discussed in the main text, though both are quite poor when summer 2024 is compared to summer 2010 (CIOA r^2 = 0.95). Opting for the 3-factor largely resulted in the CIOA diurnal profile; we have shown the CIOA profile of the 3- and 4-factor solutions plus the CalNexT CIOA in Figure 3.13. We note the dramatic change in the magnitude of the afternoon and evening CIOA peaks between the 3- and 4-factor solutions as a reason for this decision. Again, we stress that the magnitude of the difference in the total POA is negligible between the 3- and 4-factor cases, however, and do not impact the primary results of this paper.

The typical AMS/ACSM RIE for organic aerosol is 1.4, which typically holds for urban OA dominated by oxygenated OA (L. Xu et al., 2018). In this work, it is suggested that more than 50% of the OA mass is primary, and so it is possible that these reduced species have a larger RIE (Nault et al., 2023). Because the detected concentration is proportional to the inverse of the RIE, underestimating the RIE would result in an overestimation of the POA concentration. For the case of POA, this works against the conclusions of this paper. However, because we attribute a large fraction to cooking OA (CIOA), Katz and coauthors recommend a change in RIE of less than 10% (1.5 for ambient measurements), which would still leave POA the dominant contributor to the total OA (Katz et al., 2021). Further, mass closure is quite good in this study (see Figure 3.10), suggesting that an RIE for total OA of 1.4 is sufficient for the range of observed OA species.

Diurnal Cycle Analysis

When fitting the $PM_{2.5}$ data to assess the diurnal cycle, we enforce the constraint that the diurnal profile is a harmonic of order 1. In general, in the summertime AMS measurements have suggested this to be roughly accurate for PM_1 (Hayes et al., 2013; Hersey et al., 2011; Schulze et al., 2024); while the shape does not perfectly fit a sinusoidal curve, there is indeed one maximum and one minimum,

and so this approximation is to first order an accurate depiction of the real world. In the wintertime, in central LA, this approximation seems good, though in Riverside, for instance, the presence of a morning peak corresponding to rush hour could bias the fit (Ivančič et al., 2022). We additionally show this in Figure 3.14; while there is a slight bump in the morning PM, a first order sine curve can still be fit to this data to extract the timing of the nighttime maximum.
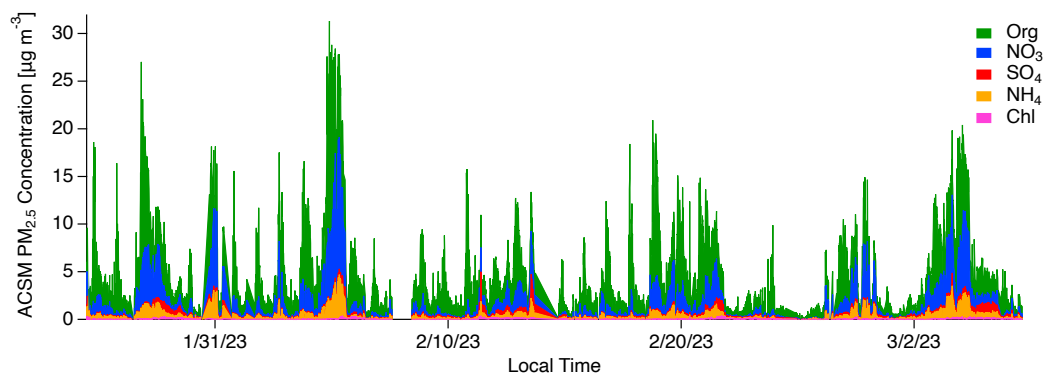
Figure 3.5: Time series of measurements during the WAQS-LA campaign.
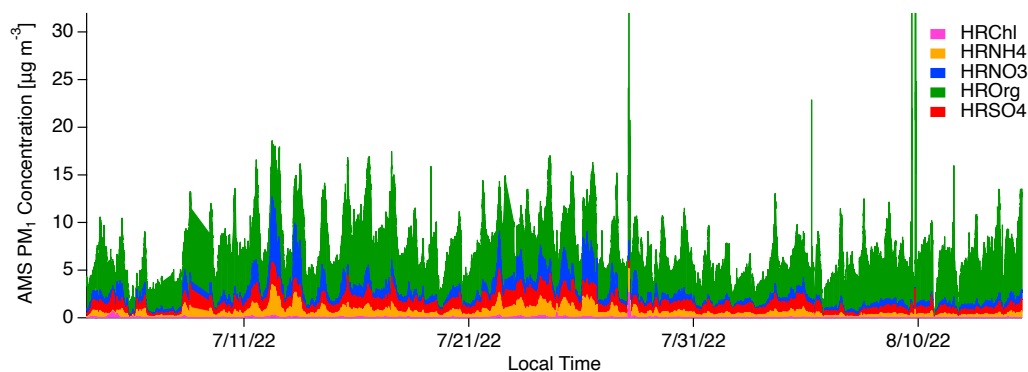
Figure 3.6: Time series of measurements during the CalNexT campaign. Reproduced from Schulze et al. (Schulze et al., 2024).
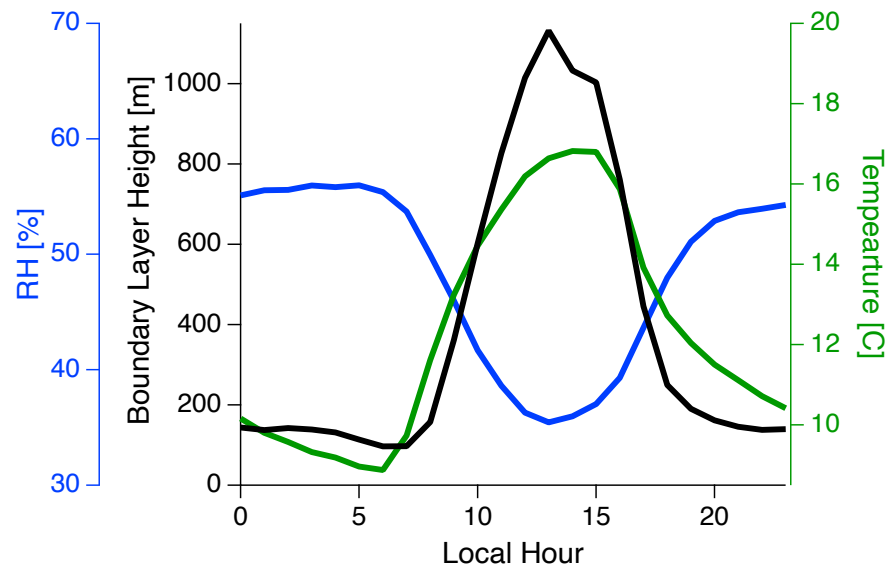
Figure 3.7: Average diunal profile of meteorological parameters during WAQS-LA. Temperature and Relative Humidity were measured during the campaign, boundary layer height is taken from reanalysis data. Axes colors correspond to their respective traces.
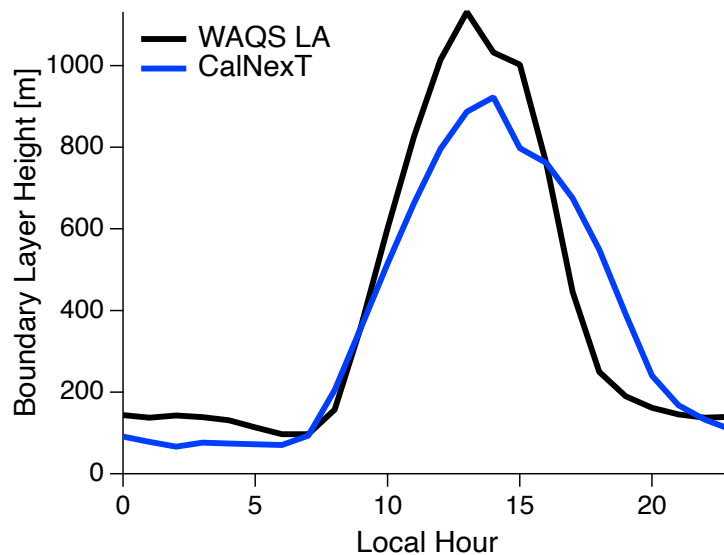
Figure 3.8: Average diurnal profiles of boundary layer height during WAQS-LA and CalNexT, taken from reanalysis data.
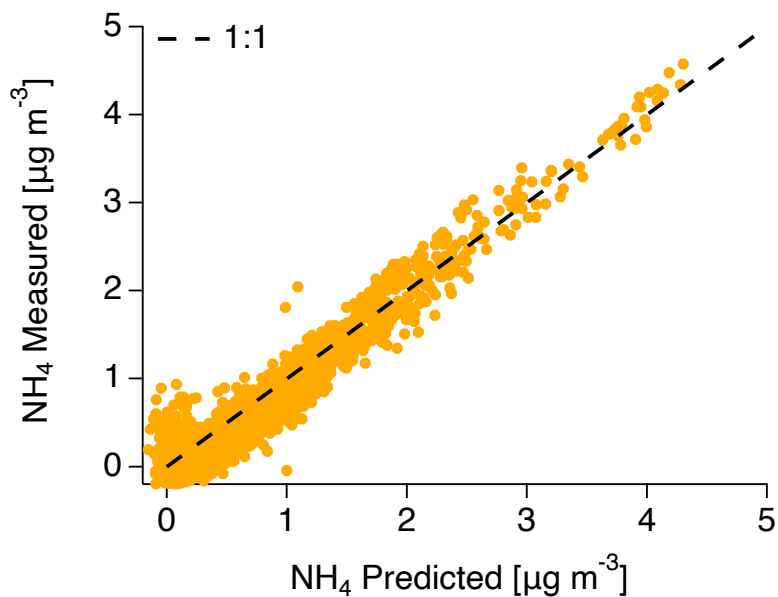
Figure 3.9: Ammonia balance for the WAQS-LA campaign. Data points represent 10 min average data. Predicted NH_4^+ is calculated as the molar equivalent of the measured SO_4^{2-}, NO_3^-, and Cl^-.
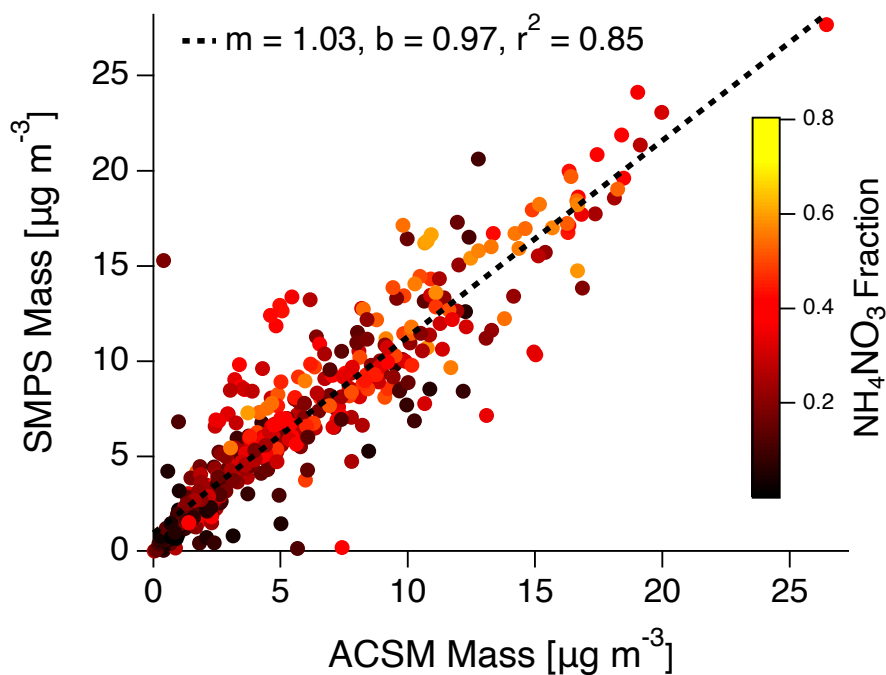
Figure 3.10: Scatter of ACSM and SMPS measurements from the WAQS-LA dataset, resampled to 10 min data. The datapoints are colored by the ACSM-derived fraction of ammonium nitrate. The dotted line represents a linear regression of the data.
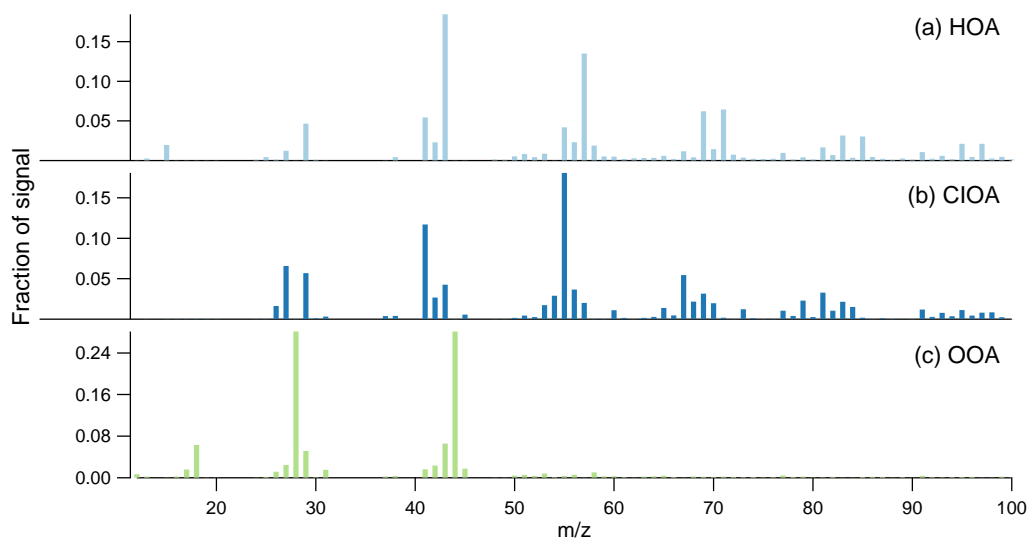
Figure 3.11: 3-factor PMF solution for the WASQ-LA data, classidied as (a) Hydrocarbon-like OA, (b) Cooking-influenced OA, and (c) Oxygenated OA. The primary OA components (POA) are colored in blue shades and the secondary OA componnets (SOA) are colored in green shades.

Figure 3.12: 4-factor PMF solution for the WASQ-LA data, classidied as (a) Hydrocarbon-like OA, (b) Cooking-Influenced OA, (c) Less-Oxidized Oxygenated OA, and (d) More-Oxidized Oxygenated OA. The primary OA components (POA) are colored in blue shades and the secondary OA components (SOA) are colored in green shades.
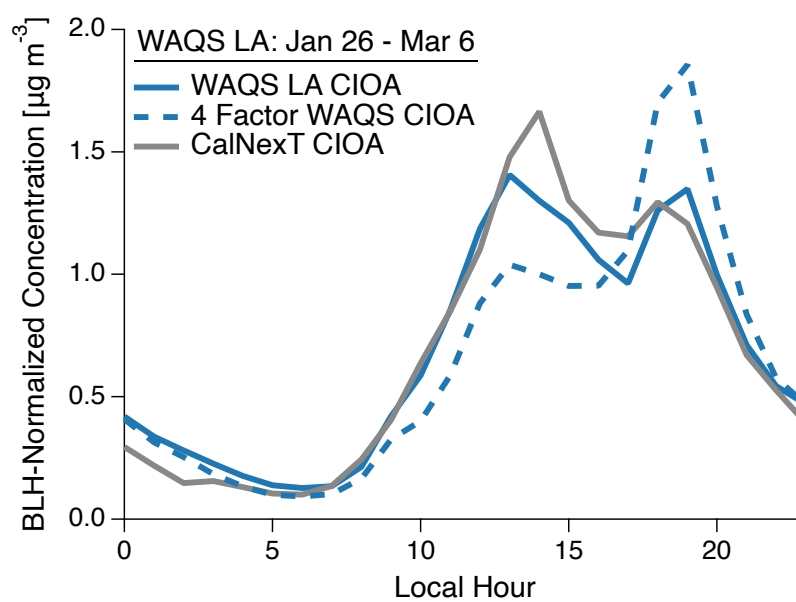
Figure 3.13: Diurnal profile of the CIOA factor normalized to the boundary layer height for the WAQS-LA 3- and 4-factor CIOA and the CalNexT CIOA. The WAQS-LA and CalNexT are reproduced from the main text.
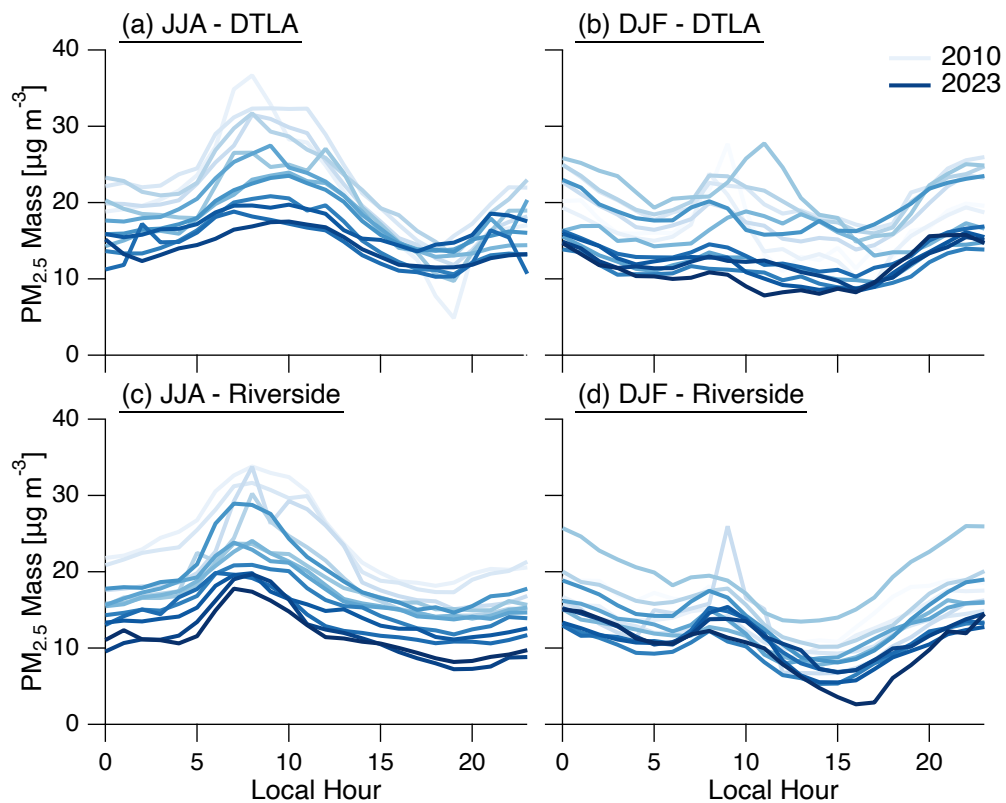
Figure 3.14: Seasonally-averaged diurnal profiles for two SCQMD monitoring sites, Downtown LA (DTLA) and Riverside, in two seasons, winter (DJF) and summer (JJA). Traces are colored by the year, starting with 2010 at the lightest intensity and ending with 2023 in the darkest intensity.

References

Canagaratna, M. R., Jimenez, J. L., Kroll, J. H., Chen, Q., Kessler, S. H., Massoli, P., Hildebrandt Ruiz, L., Fortner, E., Williams, L. R., Wilson, K. R., Surratt, J. D., Donahue, N. M., Jayne, J. T., & Worsnop, D. R. (2015). Elemental ratio measurements of organic compounds using aerosol mass spectrometry: Characterization, improved calibration, and implications. *Atmospheric Chemistry and Physics*, *15*(1), 253–272. https://doi.org/10.5194/acp-15-253-2015

Christopoulos, C., & Schneider, T. (2021). Assessing Biases and Climate Implications of the Diurnal Precipitation Cycle in Climate Models. *Geophysical Research Letters*, *48*(13). https://doi.org/10.1029/2021GL093017

Crippa, M., DeCarlo, P. F., Slowik, J. G., Mohr, C., Heringa, M. F., Chirico, R., Poulain, L., Freutel, F., Sciare, J., Cozic, J., Di Marco, C. F., Elsasser, M., Nicolas, J. B., Marchand, N., Abidi, E., Wiedensohler, A., Drewnick, F., Schneider, J., Borrmann, S., . . . Baltensperger, U. (2013). Wintertime aerosol chemical composition and source apportionment of the organic fraction in the metropolitan area of Paris. *Atmospheric Chemistry and Physics*, *13*(2), 961–981. https://doi.org/10.5194/acp-13-961-2013

DeCarlo, P. F., Kimmel, J. R., Trimborn, A., Northway, M. J., Jayne, J. T., Aiken, A. C., Gonin, M., Fuhrer, K., Horvath, T., Docherty, K. S., Worsnop, D. R., & Jimenez, J. L. (2006). Field-Deployable, High-Resolution, Time-of-Flight Aerosol Mass Spectrometer. *Analytical Chemistry*, *78*(24), 8281–8289. https://doi.org/10.1021/ac061249n

EPA. (2024). $PM_{2.5}$ (2012) Designated Area/State Information. Retrieved June 20, 2024, from https://www3.epa.gov/airquality/greenbook/kbtc.html

Farmer, D. K., Matsunaga, A., Docherty, K. S., Surratt, J. D., Seinfeld, J. H., Ziemann, P. J., & Jimenez, J. L. (2010). Response of an aerosol mass spectrometer to organonitrates and organosulfates and implications for atmospheric chemistry. *Proceedings of the National Academy of Sciences*, *107*(15), 6670–6675. https://doi.org/10.1073/pnas.0912340107

Fröhlich, R., Cubison, M. J., Slowik, J. G., Bukowiecki, N., Prévôt, A. S. H., Baltensperger, U., Schneider, J., Kimmel, J. R., Gonin, M., Rohner, U., Worsnop, D. R., & Jayne, J. T. (2013). The ToF-ACSM: A portable aerosol chemical speciation monitor with TOFMS detection. *Atmospheric Measurement Techniques*, *6*(11), 3225–3241. https://doi.org/10.5194/amt-6-3225-2013

Hasheminassab, S., Daher, N., Saffari, A., Wang, D., Ostro, B. D., & Sioutas, C. (2014). Spatial and temporal variability of sources of ambient fine particulate matter $PM_{2.5}$ in California. *Atmospheric Chemistry and Physics*, *14*(22), 12085–12097. https://doi.org/10.5194/acp-14-12085-2014

Hasheminassab, S., Daher, N., Ostro, B. D., & Sioutas, C. (2014). Long-term source apportionment of ambient fine particulate matter ($PM_{2.5}$) in the Los Angeles Basin: A focus on emissions reduction from vehicular sources. *Environmental Pollution*, *193*, 54–64. https://doi.org/10.1016/j.envpol.2014.06.012

Hass-Mitchell, T., Joo, T., Rogers, M., Nault, B. A., Soong, C., Tran, M., Seo, M., Machesky, J. E., Canagaratna, M., Roscioli, J., Claflin, M. S., Lerner, B. M., Blomdahl, D. C., Misztal, P. K., Ng, N. L., Dillner, A. M., Bahreini, R., Russell, A., Krechmer, J. E., . . . Gentner, D. R. (2024). Increasing Contributions of Temperature-Dependent Oxygenated Organic Aerosol to Summertime Particulate Matter in New York City. *ACS ES&T Air*, *1*(2), 113–128. https://doi.org/10.1021/acsestair.3c00037

Hayes, P. L., Ortega, A. M., Cubison, M. J., Froyd, K. D., Zhao, Y., Cliff, S. S., Hu, W. W., Toohey, D. W., Flynn, J. H., Lefer, B. L., Grossberg, N., Alvarez, S., Rappenglück, B., Taylor, J. W., Allan, J. D., Holloway, J. S., Gilman, J. B., Kuster, W. C., de Gouw, J. A., . . . Jimenez, J. L. (2013). Organic aerosol composition and sources in Pasadena, California, during the 2010 CalNex campaign. *Journal of Geophysical Research: Atmospheres*, *118*(16), 9233–9257. https://doi.org/10.1002/jgrd.50530

Hersbach, H., Bell, B., Berrisford, P., Biavati, G., Horányi, A., Muñoz Sabater, J., Nicolas, J., Peubey, C., Radu, R., Rozum, I., Schepers, D., Simmons, A., Soci, C., Dee, D., & Thépaut, J.-N. (2023). ERA5 hourly data on single levels from 1940 to present. https://doi.org/10.24381/cds.adbb2d47

Hersey, S. P., Craven, J. S., Schilling, K. A., Metcalf, A. R., Sorooshian, A., Chan, M. N., Flagan, R. C., & Seinfeld, J. H. (2011). The Pasadena Aerosol Characterization Observatory (PACO): Chemical and physical analysis of the Western Los Angeles basin aerosol. *Atmospheric Chemistry and Physics*, *11*(15), 7417–7443. https://doi.org/10.5194/acp-11-7417-2011

Hu, W., Campuzano-Jost, P., Day, D. A., Nault, B. A., Park, T., Lee, T., Pajunoja, A., Virtanen, A., Croteau, P., Canagaratna, M. R., Jayne, J. T., Worsnop, D. R., & Jimenez, J. L. (2020). Ambient Quantification and Size Distributions for Organic Aerosol in Aerosol Mass Spectrometers with the New Capture Vaporizer. *ACS Earth and Space Chemistry*, *4*(5), 676–689. https://doi.org/10.1021/acsearthspacechem.9b00310

Hughes, L. S., Allen, J. O., Salmon, L. G., Mayo, P. R., Johnson, R. J., & Cass, G. R. (2002). Evolution of Nitrogen Species Air Pollutants along Trajectories Crossing the Los Angeles Area. *Environmental Science & Technology*, *36*(18), 3928–3935. https://doi.org/10.1021/es0110630

Ivančič, M., Gregorič, A., Lavrič, G., Alföldy, B., Ježek, I., Hasheminassab, S., Pakbin, P., Ahangar, F., Sowlat, M., Boddeker, S., & Rigler, M. (2022). Two-year-long high-time-resolution apportionment of primary and secondary carbonaceous aerosols in the Los Angeles Basin using an advanced total

carbon–black carbon (TC-BC()) method. *Science of The Total Environment*, *848*, 157606. https://doi.org/10.1016/j.scitotenv.2022.157606

Jathar, S. H., Woody, M., Pye, H. O. T., Baker, K. R., & Robinson, A. L. (2017). Chemical transport model simulations of organic aerosol in southern California: Model evaluation and gasoline and diesel source contributions. *Atmospheric Chemistry and Physics*, *17*(6), 4305–4318. https://doi.org/10.5194/acp-17-4305-2017

Jayne, J. T., Leard, D. C., Zhang, X., Davidovits, P., Smith, K. A., Kolb, C. E., & Worsnop, D. R. (2000). Development of an Aerosol Mass Spectrometer for Size and Composition Analysis of Submicron Particles. *Aerosol Science and Technology*, *33*(1-2), 49–70. https://doi.org/10.1080/027868200410840

Jimenez, J. L., Canagaratna, M. R., Donahue, N. M., Prevot, A. S. H., Zhang, Q., Kroll, J. H., DeCarlo, P. F., Allan, J. D., Coe, H., Ng, N. L., Aiken, A. C., Docherty, K. S., Ulbrich, I. M., Grieshop, A. P., Robinson, A. L., Duplissy, J., Smith, J. D., Wilson, K. R., Lanz, V. A., . . . Worsnop, D. R. (2009). Evolution of Organic Aerosols in the Atmosphere. *Science*, *326*(5959), 1525–1529. https://doi.org/10.1126/science.1180353

Jimenez, J. L. (2003). Ambient aerosol sampling using the Aerodyne Aerosol Mass Spectrometer. *Journal of Geophysical Research*, *108*(D7), 8425. https://doi.org/10.1029/2001JD001213

Kaltsonoudis, C., Kostenidou, E., Louvaris, E., Psichoudaki, M., Tsiligiannis, E., Florou, K., Liangou, A., & Pandis, S. N. (2017). Characterization of fresh and aged organic aerosol emissions from meat charbroiling [Publisher: Copernicus GmbH]. *Atmospheric Chemistry and Physics*, *17*(11), 7143–7155. https://doi.org/10.5194/acp-17-7143-2017

Katz, E. F., Guo, H., Campuzano-Jost, P., Day, D. A., Brown, W. L., Boedicker, E., Pothier, M., Lunderberg, D. M., Patel, S., Patel, K., Hayes, P. L., Avery, A., Hildebrandt Ruiz, L., Goldstein, A. H., Vance, M. E., Farmer, D. K., Jimenez, J. L., & DeCarlo, P. F. (2021). Quantification of cooking organic aerosol in the indoor environment using aerodyne aerosol mass spectrometers. *Aerosol Science and Technology*, *55*(10), 1099–1114. https://doi.org/10.1080/02786826.2021.1931013

Kleeman, M. J., & Cass, G. R. (2001). A 3D Eulerian Source-Oriented Model for an Externally Mixed Aerosol. *Environmental Science & Technology*, *35*(24), 4834–4848. https://doi.org/10.1021/es010886m

Kuwata, M., Zorn, S. R., & Martin, S. T. (2012). Using Elemental Ratios to Predict the Density of Organic Material Composed of Carbon, Hydrogen, and Oxygen. *Environmental Science & Technology*, *46*(2), 787–794. https://doi.org/10.1021/es202525q

Ma, P. K., Zhao, Y., Robinson, A. L., Worton, D. R., Goldstein, A. H., Ortega, A. M., Jimenez, J. L., Zotter, P., Prévôt, A. S. H., Szidat, S., & Hayes, P. L. (2017). Evaluating the impact of new observational constraints on P-S/IVOC emissions, multi-generation oxidation, and chamber wall losses on SOA modeling for Los Angeles, CA. *Atmospheric Chemistry and Physics*, *17*(15), 9237–9259. https://doi.org/10.5194/acp-17-9237-2017

McDonald, B. C., De Gouw, J. A., Gilman, J. B., Jathar, S. H., Akherati, A., Cappa, C. D., Jimenez, J. L., Lee-Taylor, J., Hayes, P. L., McKeen, S. A., Cui, Y. Y., Kim, S. W., Gentner, D. R., Isaacman-VanWertz, G., Goldstein, A. H., Harley, R. A., Frost, G. J., Roberts, J. M., Ryerson, T. B., & Trainer, M. (2018). Volatile chemical products emerging as largest petrochemical source of urban organic emissions. *Science*, *359*(6377), 760–764. https://doi.org/10.1126/science.aaq0524

Middlebrook, A. M., Bahreini, R., Jimenez, J. L., & Canagaratna, M. R. (2012). Evaluation of Composition-Dependent Collection Efficiencies for the Aerodyne Aerosol Mass Spectrometer using Field Data. *Aerosol Science and Technology*, *46*(3), 258–271. https://doi.org/10.1080/02786826.2011.620041

Mohr, C., DeCarlo, P. F., Heringa, M. F., Chirico, R., Slowik, J. G., Richter, R., Reche, C., Alastuey, A., Querol, X., Seco, R., Peñuelas, J., Jiménez, J. L., Crippa, M., Zimmermann, R., Baltensperger, U., & Prévôt, A. S. H. (2012). Identification and quantification of organic aerosol from cooking and other sources in Barcelona using aerosol mass spectrometer data. *Atmospheric Chemistry and Physics*, *12*(4), 1649–1665. https://doi.org/10.5194/acp-12-1649-2012

Nault, B. A., Croteau, P., Jayne, J., Williams, A., Williams, L., Worsnop, D., Katz, E. F., DeCarlo, P. F., & Canagaratna, M. (2023). Laboratory evaluation of organic aerosol relative ionization efficiencies in the aerodyne aerosol mass spectrometer and aerosol chemical speciation monitor. *Aerosol Science and Technology*, *57*(10), 981–997. https://doi.org/10.1080/02786826.2023.2223249

Ng, N. L., Canagaratna, M. R., Jimenez, J. L., Chhabra, P. S., Seinfeld, J. H., & Worsnop, D. R. (2011). Changes in organic aerosol composition with aging inferred from aerosol mass spectra. *Atmospheric Chemistry and Physics*, *11*(13), 6465–6474. https://doi.org/10.5194/acp-11-6465-2011

Ng, N. L., Herndon, S. C., Trimborn, A., Canagaratna, M. R., Croteau, P. L., Onasch, T. B., Sueper, D., Worsnop, D. R., Zhang, Q., Sun, Y. L., & Jayne, J. T. (2011). An Aerosol Chemical Speciation Monitor (ACSM) for Routine Monitoring of the Composition and Mass Concentrations of Ambient Aerosol. *Aerosol Science and Technology*, *45*(7), 780–794. https://doi.org/10.1080/02786826.2011.560211

Nussbaumer, C. M., & Cohen, R. C. (2021). Impact of OA on the Temperature Dependence of PM$_{2.5}$ in the Los Angeles Basin. *Environmental Science & Technology*, *55*(6), 3549–3558. https://doi.org/10.1021/acs.est.0c07144

Paatero, P. (1997). Least squares formulation of robust non-negative factor analysis. *Chemometrics and Intelligent Laboratory Systems*, *37*(1), 23–35. https://doi.org/10.1016/S0169-7439(96)00044-5

Paatero, P., & Tapper, U. (1994). Positive matrix factorization: A non-negative factor model with optimal utilization of error estimates of data values. *Environmetrics*, *5*(2), 111–126. https://doi.org/10.1002/env.3170050203

Pfannerstill, E. Y., Arata, C., Zhu, Q., Schulze, B. C., Ward, R., Woods, R., Harkins, C., Schwantes, R. H., Seinfeld, J. H., Bucholtz, A., Cohen, R. C., & Goldstein, A. H. (2024). Temperature-dependent emissions dominate aerosol and ozone formation in Los Angeles. *Science*, *384*(6702), 1324–1329. https://doi.org/10.1126/science.adg8204

Pusede, S. E., Duffey, K. C., Shusterman, A. A., Saleh, A., Laughner, J. L., Wooldridge, P. J., Zhang, Q., Parworth, C. L., Kim, H., Capps, S. L., Valin, L. C., Cappa, C. D., Fried, A., Walega, J., Nowak, J. B., Weinheimer, A. J., Hoff, R. M., Berkoff, T. A., Beyersdorf, A. J., . . . Cohen, R. C. (2016). On the effectiveness of nitrogen oxide reductions as a control over ammonium nitrate aerosol. *Atmospheric Chemistry and Physics*, *16*(4), 2575–2596. https://doi.org/10.5194/acp-16-2575-2016

Rahn, D. A., & Mitchell, C. J. (2016). Diurnal Climatology of the Boundary Layer in Southern California Using AMDAR Temperature and Wind Profiles. *Journal of Applied Meteorology and Climatology*, *55*(5), 1123–1137. https://doi.org/10.1175/JAMC-D-15-0234.1

Robinson, A. L., Donahue, N. M., Shrivastava, M. K., Weitkamp, E. A., Sage, A. M., Grieshop, A. P., Lane, T. E., Pierce, J. R., & Pandis, S. N. (2007). Rethinking Organic Aerosols: Semivolatile Emissions and Photochemical Aging. *Science*, *315*(5816), 1259–1262. https://doi.org/10.1126/science.1133061

Schauer, J. J., Rogge, W. F., Hildemann, L. M., Mazurek, M. M., Cass, G. R., & Simoneit, B. R. T. (1996). Source apportionment of airborne particulate matter using organic compounds as tracers. *Atmospheric Environment*, *30*(22).

Schulze, B. C., Kenseth, C. M., Ward, R. X., Pennington, E. A., Rooy, P. V., Tasnia, A., Barletta, B., Meinardi, S., Morris, M., Jensen, A., Huang, Y., Parker, H. A., Hasheminassab, S., Day, D., Campuzano-Jost, P., de Gouw, J., Jimenez, J. L., Barsanti, K. C., Pye, H. O. T., . . . Seinfeld, J. H. (2024). Insights into the complex effects of reduced mobile source emissions on. *To Be Submitted*.

Schulze, B. C., Ward, R. X., Pfannerstill, E. Y., Zhu, Q., Arata, C., Place, B., Nussbaumer, C., Wooldridge, P., Woods, R., Bucholtz, A., Cohen, R. C., Goldstein, A. H., Wennberg, P. O., & Seinfeld, J. H. (2023). Methane Emissions from Dairy Operations in California's San Joaquin Valley Evaluated Using Airborne Flux Measurements. *Environmental Science & Technology*, *57*(48), 19519–19531. https://doi.org/10.1021/acs.est.3c03940

Seinfeld, J. H., & Pandis, S. N. (2016). *Atmospheric Chemistry and Physics: From Air Pollution to Climate Change*. Wiley & Sons.

Shrivastava, M. K., Lipsky, E. M., Stanier, C. O., & Robinson, A. L. (2006). Modeling Semivolatile Organic Aerosol Mass Emissions from Combustion Systems. *Environmental Science & Technology*, *40*(8), 2671–2677. https://doi.org/10.1021/es0522231

Sun, P., Farley, R. N., Li, L., Srivastava, D., Niedek, C. R., Li, J., Wang, N., Cappa, C. D., Pusede, S. E., Yu, Z., Croteau, P., & Zhang, Q. (2022). $PM_{2.5}$ composition and sources in the San Joaquin Valley of California: A long-term study using ToF-ACSM with the capture vaporizer. *Environmental Pollution*, *292*, 118254. https://doi.org/10.1016/j.envpol.2021.118254

Sun, Y.-L., Zhang, Q., Schwab, J. J., Demerjian, K. L., Chen, W.-N., Bae, M.-S., Hung, H.-M., Hogrefe, O., Frank, B., Rattigan, O. V., & Lin, Y.-C. (2011). Characterization of the sources and processes of organic and inorganic aerosols in New York city with a high-resolution time-of-flight aerosol mass apectrometer. *Atmospheric Chemistry and Physics*, *11*(4), 1581–1602. https://doi.org/10.5194/acp-11-1581-2011

Tuet, W. Y., Chen, Y., Xu, L., Fok, S., Gao, D., Weber, R. J., & Ng, N. L. (2017). Chemical oxidative potential of secondary organic aerosol (SOA) generated from the photooxidation of biogenic and anthropogenic volatile organic compounds. *Atmospheric Chemistry and Physics*, *17*(2), 839–853. https://doi.org/10.5194/acp-17-839-2017

Verma, V., Fang, T., Xu, L., Peltier, R. E., Russell, A. G., Ng, N. L., & Weber, R. J. (2015). Organic Aerosols Associated with the Generation of Reactive Oxygen Species (ROS) by Water-Soluble $PM_{2.5}$. *Environmental Science & Technology*, *49*(7), 4646–4656. https://doi.org/10.1021/es505577w

Wang, Y., Xiao, S., Zhang, Y., Chang, H., Martin, R. V., Van Donkelaar, A., Gaskins, A., Liu, Y., Liu, P., & Shi, L. (2022). Long-term exposure to $PM_{2.5}$ major components and mortality in the southeastern United States. *Environment International*, *158*, 106969. https://doi.org/10.1016/j.envint.2021.106969

Ware, J., Kort, E. A., DeCola, P., & Duren, R. (2016). Aerosol lidar observations of atmospheric mixing in Los Angeles: Climatology and implications for greenhouse gas observations. *Journal of Geophysical Research: Atmospheres*, *121*(16), 9862–9878. https://doi.org/10.1002/2016JD024953

Warneke, C., De Gouw, J. A., Edwards, P. M., Holloway, J. S., Gilman, J. B., Kuster, W. C., Graus, M., Atlas, E., Blake, D., Gentner, D. R., Goldstein, A. H., Harley, R. A., Alvarez, S., Rappenglueck, B., Trainer, M., & Parrish, D. D. (2013). Photochemical aging of volatile organic compounds in the Los Angeles basin: Weekday-weekend effect. *Journal of Geophysical Research: Atmospheres*, *118*(10), 5018–5028. https://doi.org/10.1002/jgrd.50423

Womack, C. C., McDuffie, E. E., Edwards, P. M., Bares, R., De Gouw, J. A., Docherty, K. S., Dubé, W. P., Fibiger, D. L., Franchin, A., Gilman, J. B., Goldberger, L., Lee, B. H., Lin, J. C., Long, R., Middlebrook, A. M., Millet, D. B., Moravek, A., Murphy, J. G., Quinn, P. K., . . . Brown, S. S. (2019). An Odd Oxygen Framework for Wintertime Ammonium Nitrate Aerosol Pollution in Urban Areas: NO $_x$ and VOC Control as Mitigation Strategies. *Geophysical Research Letters*, *46*(9), 4971–4979. https://doi.org/10.1029/2019GL082028

Wyzga, R., & Rohr, A. (2015). Long-term particulate matter exposure: Attributing health effects to individual PM components. *Journal of the Air & Waste Management Association*, *65*(5), 523–543. https://doi.org/10.1080/10962247.2015.1020396

Xu, L., Suresh, S., Guo, H., Weber, R. J., & Ng, N. L. (2015). Aerosol characterization over the southeastern United States using high-resolution aerosol mass spectrometry: Spatial and seasonal variation of aerosol composition and sources with a focus on organic nitrates [Publisher: Copernicus GmbH]. *Atmospheric Chemistry and Physics*, *15*(13), 7307–7336. https://doi.org/10.5194/acp-15-7307-2015

Xu, L., Pye, H. O. T., He, J., Chen, Y., Murphy, B. N., & Ng, N. L. (2018). Experimental and model estimates of the contributions from biogenic monoterpenes and sesquiterpenes to secondary organic aerosol in the southeastern United States. *Atmospheric Chemistry and Physics*, *18*(17), 12613–12637. https://doi.org/10.5194/acp-18-12613-2018

Xu, W., Croteau, P., Williams, L., Canagaratna, M., Onasch, T., Cross, E., Zhang, X., Robinson, W., Worsnop, D., & Jayne, J. (2017). Laboratory characterization of an aerosol chemical speciation monitor with PM $_{2.5}$ measurement capability. *Aerosol Science and Technology*, *51*(1), 69–83. https://doi.org/10.1080/02786826.2016.1241859

Zhang, Q., Jimenez, J. L., Canagaratna, M. R., Allan, J. D., Coe, H., Ulbrich, I., Alfarra, M. R., Takami, A., Middlebrook, A. M., Sun, Y. L., Dzepina, K., Dunlea, E., Docherty, K., DeCarlo, P. F., Salcedo, D., Onasch, T., Jayne, J. T., Miyoshi, T., Shimono, A., . . . Worsnop, D. R. (2007). Ubiquity and dominance of oxygenated species in organic aerosols in anthropogenically-influenced Northern Hemisphere midlatitudes. *Geophysical Research Letters*, *34*(13), 2007GL029979. https://doi.org/10.1029/2007GL029979

Zhang, Q., Jimenez, J. L., Canagaratna, M. R., Ulbrich, I. M., Ng, N. L., Worsnop, D. R., & Sun, Y. (2011). Understanding atmospheric organic aerosols via factor analysis of aerosol mass spectrometry: A review. *Analytical and Bioanalytical Chemistry*, *401*(10), 3045–3067. https://doi.org/10.1007/s00216-011-5355-y

Zhao, Y., Tkacik, D. S., May, A. A., Donahue, N. M., & Robinson, A. L. (2022). Mobile Sources Are Still an Important Source of Secondary Organic Aerosol and Fine Particulate Matter in the Los Angeles Region. *Environmental Science & Technology*, *56*(22), 15328–15336. https://doi.org/10.1021/acs.est.2c03317

Chapter 4

CLARIFYING THE IMPORTANCE OF SURFACE-ACTIVE ORGANICS IN BIOGENIC CCN

Ryan X. Ward, Benjamin C. Schulze, Yuanlong Huang, Richard C. Flagan, and John H. Seinfeld

4.1 Abstract

Multiple studies suggest that surface-active organic species can depress the surface tension of aerosol particles if partitioned to the surface, in turn enhancing their propensity to serve as CCN. The conventional parameterization of aerosol hygroscopicity used for atmospheric modeling, κ-Köhler theory, prescribes a constant surface tension (equal to that of water), and is thus unable to capture this behavior. It has been shown that monoterpene and sesquiterpene oxidation products, which exhibit a range of biogenic SOA hygroscopicities, can depress surface tension of bulk solutions below that of water, suggesting this phenomenon could be important in the aerosol phase. Considering the abundance of biogenic SOA and its substantial contribution to the global CCN budget, the omission of surface tension effects could pose important impacts to modeling the climate-relevant behavior of these species. In this work, we first examine surface tension effects with a flow tube reactor; α-pinene and β-caryophyllene SOA seeded by ammonium sulfate are generated, and by varying particle size, organic mass fraction, and oxidative age, a characterization of hygroscopicity is made. To capture the surface partitioning of the organics, a thermodynamic compressed film framework is fit to the lab results and is shown to accurately describe the deviations from κ-Köhler theory, suggesting indirectly the presence of surface effects. In turn, we contextualize this compressed film framework with ambient data to rationalize the importance of surface tension effects in understanding real-world aerosol. Our results provide insight into the physicochemical detail needed to accurately represent biogenic SOA CCN activation in regional and global models.

4.2 Introduction

It has been known for decades that atmospheric aerosols play an important role in climate by serving both as scatterers of solar radiation and as the nuclei upon which

clouds form (Seinfeld & Pandis, 2016; Twomey, 1974). To this second point, the extent to which particle size and composition, and in turn the resulting physcio-chemical properties, affect an aerosol's propensity to serve as a cloud condensation nuclei (CCN) has been the subject of many decades of research. It is common to parameterize this behavior by hygroscopicity (κ), which is a catch-all parameter describing how the particle's physicochemical properties influence water uptake (Petters & Kreidenweis, 2007). In combining this parameter with the physics of droplet activation, the so-called κ-Köhler framework has been useful for assessing the impact of aeroosl properties on clouds (Farmer et al., 2015).

One key assumption to the κ-Köhler framework is that that the aerosol, and in turn the cloud droplet, maintains the surface tension of water over the activation process. For a dilute aqueous aerosol, primarily of inorganic constituents, this assumption is reasonable. In the case of organic aerosol, it is possible that organic species may be surface-active and act as surfactants, lowering the surface tension of the droplet by up to a factor of two or more (Davies et al., 2018; Ruehl & Wilson, 2014). In lowering the surface tension, the critical supersaturation of water required to activate the aerosol is lowered, which enhances the CCN activity of the aerosol. However, if the organic phase partitions to the surface from the bulk of the aerosol, it is not unreasonable to think that the increase in water activity may offset this change in surface tension (see Supporting Information for detailed discussion) (Wang et al., 2019). Furthermore, the extent to which this interplay affects cloud droplet number concentration is not clear due to the complexity of this behavior, and creating a model which can capture the behavior of aerosol thermodynamics at the tens of nanometer scale while resolving clouds at the meters scale is not trivial.

Despite this physciochemical complexity, ambient observations and model studies have linked surface-active organic aerosol with increased CCN activity (Ovadnevaite et al., 2017; Sareen et al., 2017). Consequently, many laboratory and experimental studies have tried to assess the implications of phase partitioning on CCN activity. Bulk solution and aerosol-phase measurements have suggested a lower surface tension (Gray Bé et al., 2017), consistent with an increased CCN activity, but other work has suggested that organic coatings may actually prevent hygroscopic growth (Asa-Awuku et al., 2009; Li et al., 2021). This surface behavior is complex; it has been studied extensively in the context of reactive uptake of organic species and the ensuing changes in phase state of the particle (Lei et al., 2022; Olson et al., 2019; Shiraiwa et al., 2013). In the case that the organics depress surface tension

and enhance CCN activity, modeling studies have shown that the at high organic fractions, effects on cloud properties may be substantial (Lowe et al., 2019; Sareen et al., 2013).

One specific case where surface-active organics may be important is in the high latitude, Northern Hemisphere boreal forests (Lowe et al., 2019). Secondary organic aerosol of biogenic origin dominates the aerosol population, and therefore the CCN population, in this region as measured in Hyytiälä, Finland (Heikkinen et al., 2020, 2021). Additionally, recent studies suggest robust feedbacks between the emissions of biogenic VOCs, secondary aerosol, and cloud formation (Petäjä et al., 2022; Yli-Juuti et al., 2021). In these regions, monoterpenes are the most abundantly emitted VOC, particularly α-pinene (Hakola et al., 2012). Another important class of VOCs are sesquiterpenes, of which β-caryophyllene is the most dominant (Hakola et al., 2006). While it is emitted in smaller quantities than α-pinene, β-caryophyllene is highly reactive with OH and O_3, and its SOA mass yield can be substantially higher than that of α-pinene (Pathak et al., 2007; Tasoglou & Pandis, 2015; Winterhalter et al., 2009). Bulk laboratory measurements (i.e., at length scales » than hundreds of nm) have suggested that oxidation products of α-pinene and β-caryophyllene have surface tensions lower than that of water, priming them both as candidates for surface-active organic species (Gray Bé et al., 2017).

In this work, we generate and measure the hygroscopicity of SOA derived from the oxidation of α-pinene and β-caryophyllene. Using a thermodynamic compressed film framework, we find deviations in the κ measurement consistent with a surface-active organic phase. Finally, we discuss the implications of this for understanding cloud processes in the boreal regions.

4.3   Materials and Methods

Aerosol Generation

In broad terms, the goal of the laboratory experiments was to generate mixed ammonium-sulfate-SOA of varying organic mass fraction by tuning the ratio of the seed and amount of SOA condensed. An experimental schematic is presented in the Supporting Information (Figure 4.20). SOA from either β-caryophyllene or α-pinene were generated in the Caltech Photooxidation Flow Tube reactor (CPOT), a steady-state flow tube reactor (Huang et al., 2017). All SOA was seeded by ammonium sulfate aerosol, which was size-selected by a DMA (TSI Model 3010) to a monodisperse distribution, deliquesced by a desiccant drier, and injected to

the reactor. The VOC precursors were injected into the flow tube with the seed, and oxidized, wherein the oxidation products partitioned to the particle phase (i.e., condensed onto the ammonium sulfate seed particles). At the outlet of the reactor, the particles were size-selected again by a DMA, which allowed control of the ratio of organic SOA to inorganic seed. The range of influent monodisperse particles was 30 - 50 nm, and the range of effluent coated diameters sElected for was $80 - 110$ nm. The SOA was produced via two oxidative conditions: an ozone initiated oxidation (herein "dark ozonolysis") or an OH-initiated oxidiation (herein "photoxidation").

For the case of dark ozonolysis, ozone in excess of hundreds of ppb was introduced to the reactor at RH < 10%. OH was not scrubbed from the reactor, though not expected to be present in large enough quantities to out-compete the ozone reaction. For the case of photooxidation, OH was produced in a similar manner: ozone was introduced to the reactor in the presence of water (RH in excess of 20%), and the UV lights were used to produce OH.

To measure the hygroscopicity of the generated aerosol, a Droplet Measurement Technologies (DMT) dual-column streamwise thermal-gradient cloud condensation nuclei counter (CCNC) was used, and its operating principles have been described elsewhere (Lance et al., 2006; Roberts & Nenes, 2005; Schulze et al., 2020). To extract κ, the CCNC and a condensation particle counter (CPC) are used in parallel to generate the CCN efficiency spectrum, from which the critical supersaturation can be extracted and used to infer κ. Because the aerosol are composed of only ammonium sulfate and SOA, the measured hygroscopicity is simply the volume-weighted average of the particle's constituents:

$$\kappa_{meas} = f_{org}\kappa_{org} + (1 - f_{org})\kappa_{AS} \tag{4.1}$$

where κ_{meas} is the measured hygroscopicity, f_{org} is the volume fraction of organics in the particle, κ_{AS} is the hygroscopicity of ammonium sulfate (0.61) (Petters & Kreidenweis, 2007), and κ_{org} is the hygroscopicity of the SOA. This assumption of linearity in a multi-component system is known as the Zdanovskii, Stokes, and Robinson (ZSR) assumption.

SOA Composition

The chemical composition for the various SOA-oxidation conditions was analyzed through an Aerodyne HR-ToF-AMS (Aerosol Mass Spectrometer) (DeCarlo et al., 2006; Jayne et al., 2000). Primarily, this measurement was used to determine

the O:C ratio of the effluent SOA, calculated via the "Improved-Ambient" Method (Canagaratna et al., 2015). It is important to note that for the scope of this study, we are not interested in understanding how changes in O:C drive changes in κ, but rather we are interested in understanding how SOA populations with different chemical compositions influence surface activity, and in turn how these chemical changes manifest themselves as physical changes in cloud properties. The mass spectra for the different oxidative conditions are available in the Supporting Information.

The aerosol density is inferred from the AMS measurements. The organic aerosol density is inferred from the elemental ratios, and the ratio of ammonium sulfate (fixed density) to SOA (inferred density) are used to calculate the aggregate aerosol density (Hu et al., 2020; Kuwata et al., 2012).

Measurement Uncertainty Quantification

To understand the error on the measured hygroscopicity, we need to understand the contributed errors primarily from the two DMAs (used for setting organic volume fraction) and from the CCNC (used for determining κ). It is not trivial to propagate error analytically, so measurement uncertainty is assigned through a Monte Carlo approach which has been previously employed in this context (Schulze et al., 2020; Wang et al., 2019). For clarity, we describe this process in detail.

The goal is to assign error to three quantities: the organic volume fraction (f_{org}), the hygroscopicity (κ), and the inferred organic hygroscopicity (κ_{org}). However, these quantities are not explicitly measured, but rather inverted from instrument data and calculated. So, we must start with more fundamental measurements. In the case of the DMAs we are interested in the selected diameter and calculate f_{org} as:

$$f_{org} = \frac{d_{coat}^3 - d_{seed}^3}{d_{coat}^3} \tag{4.2}$$

where d_{seed} is the mean equivalent electrical mobility diameter of the monodisperse, ammonium sulfate distribution added at the inlet of the flow tube, and d_{coat} is the diameter of the SOA-coated aerosol selected from the polydispersed aerosol population at the outlet of the flow tube. In the case of the CCNC, the quantity we infer is the critical supersaturation (S_{crit}), which we extract from the CCN efficiency spectrum given by Equation (1) in Rose et al., with corrections made as necessary (e.g., for doubly charged particle) (Rose et al., 2008). In essence, we will map these intermediate instrumental uncertainties onto the final reported measurements.

Each of these quantities (d_{seed}, d_{coat} and S_{crit}) represent surrogates for the error introduced from each instrument.

Uncertainty for each data point is calculated individually. For each of our three 'measured' quantities, we assign a normal distribution to each data point (each scatter point in Figure 4.1), taking the mean of the distribution as the measurement and the full width at half maximum (FWHM) as assigned by the errors associated with the instrument. For DMAs, the error on the size is related to the DMA resolution, the error generally goes as 1 over the resolution. For the CCNC, the error on S_{crit} is taken from the calibration reported by Schulze and colleagues (roughly 9%), though the final error appears relatively insensitive to this value compared to the error on f_{org} (Schulze et al., 2020). It is also of note that this error is more conservative than that reported by Rose and colleagues (Rose et al., 2008).

From each of these distributions, we draw a value randomly and we calculate the values that would have been 'measured' for f_{org}, κ, and κ_{org}. For the purposes of this error analysis, a more simple calculation for κ is made to save computational expense. This is described in Petters & Kreidenweis as:

$$\kappa = \frac{4}{27} \left(\frac{4\sigma M_w}{RT\rho_w} \right)^3 \left(d_{dry}^3 \ln^2 S_{crit} \right)^{-1} \tag{4.3}$$

where σ is the surface tension, M_w is the molecular weight of water, R is the ideal gas constant, T is the temperature, ρ_w is the density of water, d_{dry} is the particle size, and S_{crit} is the critical supersaturation. We are explicitly assuming that the spread in hygroscopicities would match that if we inverted the full parameterization. We repeat this process 10,000 times, which gives us distributions for each of our final independent measurements, and to these distributions we can use a Gaussian Fit to extract the variance. We take this to be the total instrument error for each measurement, and we use this error in our Markov Chain Monte Carlo fits to the compressed film model (described later).

The standard error on the data are also calculated. For each mesasurement of f_{org}, there are two independent measures of κ (the CCNC in this study has two columns). The data are then binned by f_{org} and the standard error of the bin is assigned. These discrete bins allow us to compare the representatives of the measurement data across the spectrum of organic volume fractions measured, and further allow us to explore the measurement errors relative to each other.

Thermodynamic Model

To model the influence of surface-partitioning on surface tension and, in turn, hygroscopicity, a compressed film framework was fit to the experimental results (Forestieri et al., 2018; Ruehl et al., 2016). In short, this model applies an equation-of-state and an isotherm to determine the partitioning of organics between the bulk (dissolved) phase of the aerosol, and a surface film. This allows for two important features: (1) a direct calculation of surface tension assuming organics, not water, are at the surface of the particles, and (2) a direct calculation of water activity given that not all organics are dissolved into the bulk phase. The latter point is important: it has been suggested that the effects of a depressed surface tension may be countered by Raoult's effect (Salameh et al., 2016; Seinfeld & Pandis, 2016; Wang et al., 2019), but here we can account quantitatively for these compensating effects. The model parameters are fit for four cases (β-caryophyllene or α-pinene SOA generated by either ozonolysis or photooxidation) by Markov Chain Monte Carlo. The relevant equations and description of the optimization are provided in the supplement.

Field Data

We provide atmospheric context for our data from field measurements of aerosol in two locations: a boreal forest location (Hyytiälä, Finland) and a remote marine location (Mace Head, Ireland). In the former case, measurements were made by an Aerosol Chemical Speciation Monitor (ACSM), and in the latter by AMS (Dall'Osto et al., 2010; Heikkinen et al., 2020). From these data, we infer relevant quantities, such as aerosol density, from the techniques already described.

Parcel Modeling

To provide atmospheric context to the data, the experimental results were embedded into a cloud parcel model to assess their impact on cloud properties. In particular, we are interested in a model which can not only capture the aerosol population, but also allows for surface-partitioning of organics. In the simplest case, we employ an adiabatic parcel with a fixed updraft velocity, aerosol size distribution, and specified chemical composition, and this model is described elsewhere (Schulze et al., 2020; Seinfeld & Pandis, 2016). To induce surface tension effects, we increase κ by the measurements here (see Results for discussion).
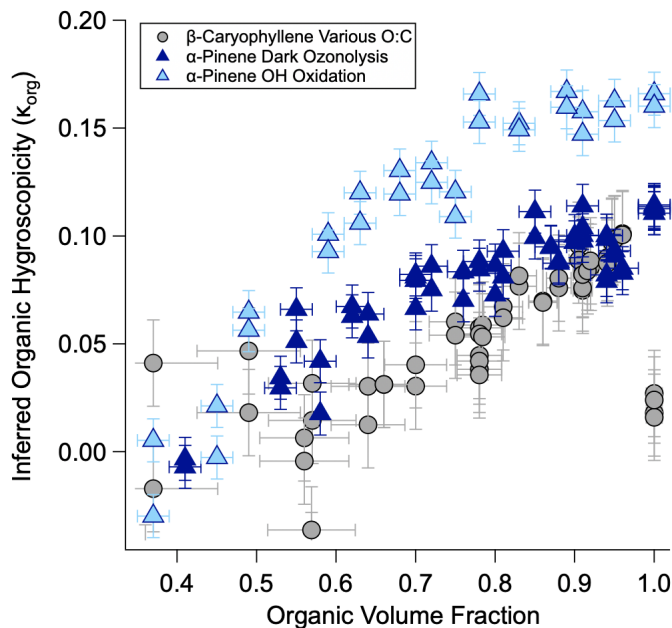
Figure 4.1: All experimental data for the two VOC and oxidative conditions. κ_{org} is inferred by Equation 4.1 and the Organic Volume Fraction (f_{org}) is calculated by Equation 4.2.

4.4   Results and Discussion

Hygroscopicity Measurements

Presented in Figure 4.1 are the hygroscopicity measurements for all the experiment. The β-caryophyllene SOA data are lumped for their oxidative conditions, which do not show distinct hygroscopicity differences, and the α-pinene SOA data are shown for their respective oxidative conditions. Each data point represents an individual experiment (that is, one combination of a monodisperse seed particle injected to the reactor, and one size-selected SOA-coataed particle at the outlet). So, for each data point, a CCN efficiency spectrum is calculated (see Methods). While the hygroscopicity of the mixed ammonium sulfate SOA was measured, we have shown the inferred κ of the organic component (inferred via equation (4.1)). For reference, for a single species this is an intensive property of a material, meaning it should not change depending on the amount of the substance present, contradicting this data set. While in our case we do not have a single species, as SOA contains a variety of species, we do have a constant composition that is uniform across the experiment, and so κ should still be a constant (a volume-weighted average of the individual κ's for each species present).
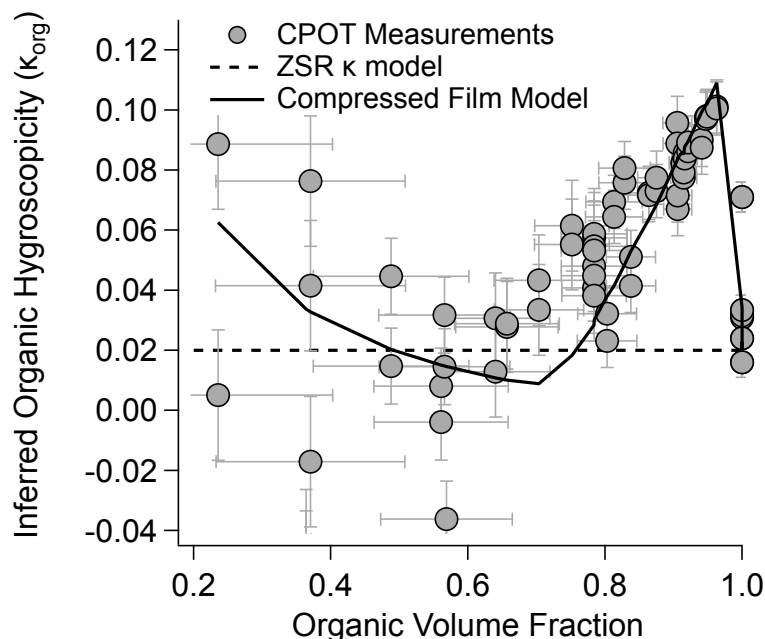
Figure 4.2: Individual measurements of hygroscopicity for β-caryophyllene SOA as a result of dark ozonolysis for various organic volume fractions (f_{org}) (same as in Figure 4.1). The dashed line represents the intrinsic hygroscopicty of β-caryophyllene, taken from the f_{org}=1 measurements. The solid line is a fit of the data taken from the compressed film model.

Most prominently, we observed large enhancements in κ_{org} at large organic volume fractions, where the expected value of hygroscipicity is enhanced by more than a factor five over the value expected by the ZSR mixing assumed in the κ-Köhler framework. We observed this trend for both VOC and oxidation types, shown in Figure 4.1. We highlight the β-caryophyllene dark ozonolysis data in Figure 4.2; of note is the a discontinuity in the κ_{org} data at an organic volume fraction of 1. For reference, the intrinsic hygroscopicity of pure β-caryophyllene SOA is plotted as $\kappa = 0.02$ (dashed), which is based on our own measurements and agrees well with previously reported values. This is likely an upper bound, as it has been reported as low as 0.001 (Frosch et al., 2013), and so we attribute the discontinuity a lack of water uptake with no electrolytes present in the particle to foster hygroscopic growth.

For the OH-initiated oxidation of β-caryophyllene, the SOA do not produce a substantially different trend than the SOA generated from dark ozonolysis. This contrasts the results of α-pinene, where there is a notable increase in the inferred organic hygroscopicity under the OH-initiated SOA compared to the ozone-initiated SOA.

Thermodynamic Modeling

The laboratory data were fit to the compressed film model for each of the 4 oxidation/VOC combinations, extracting the parameters A_0 (critical molecular area), m_σ (surface interaction parameter), $\log C_0$ (bulk concentration), and σ_{min} (effectively, the surface tension of the organics). The fits inferred an apparent κ (and therefore κ_{org}) from the critical supersaturation of an aerosol particle exhibiting surface tension effects over the course of its activation. Three cases were fit: (1) the Molecular Weight (MW) was not a free parameter (see Supporting Information for SOA MWs); (2) the MW was a free parameter, and (3) MW and minimum surface tension were fixed. These results are shown in Table 4.1. Corner plots of results are included in the Supporting Information.

Briefly, MW is scaled by O:C, a calculation parameterized by the results of α-pinene chamber studies (Claflin et al., 2018). MW is taken as monotonic in O:C, thereby increasing with oxidation, which may not be the case. The minimum surface tension, when fixed, was set to 40 mJ m^{-2}, which would be a lower bound suggested by bulk measurements (Gray Bé et al., 2017).

In general, the fits suggest the model is overparameterized to the data: the fits do not always generate Gaussian posterior parameter distributions, instead showing multimodal parameter solutions. Nonetheless, the fits, an instance of which is shown in Figure 4.2, track the data well. That the compressed film model can accurately represent the hygroscopicty measurements in the data suggests that surface tension depression is a possible mechanistic explanation for the enhanced κ_{org}. Again, it should be stressed that this is an indirect link; surface tension was not measured in the aerosol-phase in this study.

There is likely a lot to be learned by comparison of these parameters, which are related to fundamental aerosol parameters (e.g., surface tension), for various compounds. For instance, oleic acid, a C-18 aliphatic compound, was reported by Forestieri and coworkers to have a critical molecular area (A_0) of 48.5, which is substantially lower than any of the fit parameters in this work. Recall that our work covers C-10 and C-15 precursor VOCs, and to the extent that the SOA is not dominated by fragmentation, we should expect a large fraction of the SOA to retain a Carbon number near those two values. Though we recommend caution in comparing to our fit results, it is surprising that the oleic acid fit is even smaller than what Ruehl and colleagues report for the critical area of malonic acid, a C-3 compound (Forestieri et al., 2018; Ruehl et al., 2016). While uncertainties are reported in these

Table 4.1: Parameters extracted from MCMC runs on the data in this work, in addition to parameter extractions for other species in other studies.

Study	Organic Species	A_0 (Å²)	m_σ (mK m⁻² Å⁻²)	log C_0	σ_{min} (mJ m⁻²)	MW (g mol⁻¹)
This work[1]	β-cary + O_3	101.81	0.5	-6.86	30	298.6
	β-cary + OH	129.07	0.48	-4.74	37	359.9
	α-pin + O_3	99.07	0.77	-3.62	50	209.3
	α-pin + OH	124.48	0.87	-1.96	39	264.9
This work, fit MW	β-cary + O_3	94.13	0.55	-7.26	29	279
	β-cary + OH	104.06	0.44	-3.95	44	251
	α-pin + O_3	71.98	0.85	-3.09	36	156
	α-pin + OH	81.46	0.73	-2.32	54	122
This work, iso σ^2	β-cary + O_3	101.17	0.38	-0.41	40	298.6
	β-cary + OH	126.85	0.26	-5.2	40	359.9
	α-pin + O_3	77.89	0.44	-2.41	40	209.3
	α-pin + OH	142.47	0.23	-4.95	40	264.9
Forestieri et al. 2018	Oleic Acid	48.5	2.15	-6.1	34.5	282.47
	Myristic acid	29.2	1.28	-7.4	–	228.37
	Oleic and Palmitic	35.2	5.41	-5.24	28.4	–
Ruehl et al. 2016	Malonic Acid	71.2	1.13	-6.1	32.4	104.0615
	Succinic Acid	76.9	1.04	-6.2	35.4	118.09
	Glutaric Acid	62	1.06	-7	30	132.12
	Pimelic Acid	95	0.66	-6	46	160.17
	Subteric Acid	210	1	-9	46	174.2

[1] MW held constant.
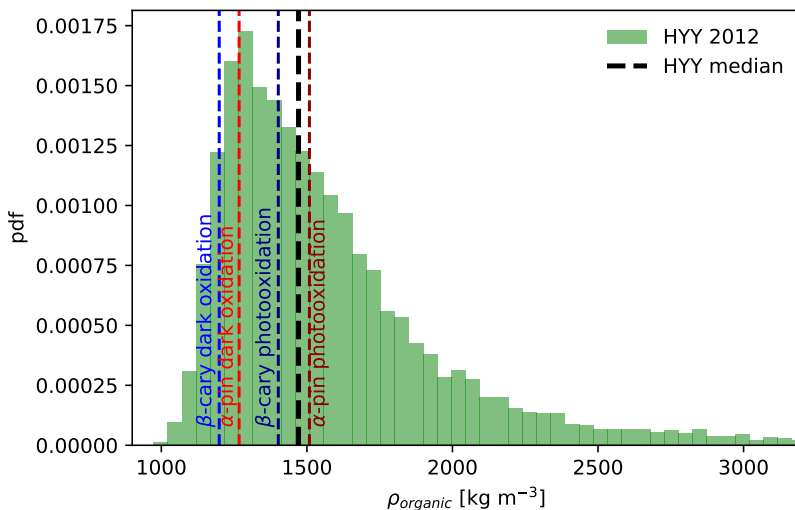[2] Surface tension and MW held constant.

Figure 4.3: Probability density function (PDF) of densities observed in Hyytiälä during 2012 inferred from ACSM measurements. SOA densities observed in this study are overlain.

studies (of order $< \pm 5$ Å for A_0), it is unclear how these are calculated in either study, and based on our work, the convergence of this model is not trivial.

Interestingly, when MW is a free parameter in our study, the fitted MW is lower at both higher O:C conditions, contrasting our expectation based on parameterized relationship between O:C and MW. However, the lack of convergence in our MCMC suggests this may not be the true value. We find, on the whole, that $\log C_0$ expresses a large degree of control on the system, and further work should target an array of optimizations on this parameter to try and ascertain its true value.

Atmospheric Implications

To test the representativeness of the lab-generated SOA, we compared with real-world data from a boreal region. In Figure 4.3, we have overlain the estimated densities of the lab-generated SOA with a PDF of ambienntly observed OA density from Hyytiälä, Finland. We observe that between the four cases, our SOA generally fall within the range of observed OA, suggesting that the chemical identities of the lab and ambient OA are similar.

With this in mind, we sought to compare the utility of the compressed film framework in understanding errors in κ in the case that surface tension depression is occurring. In other words, are there sufficient errors in κ generated when surface-active organics are or are not taken into account? For a variety of combinations of inorganic and
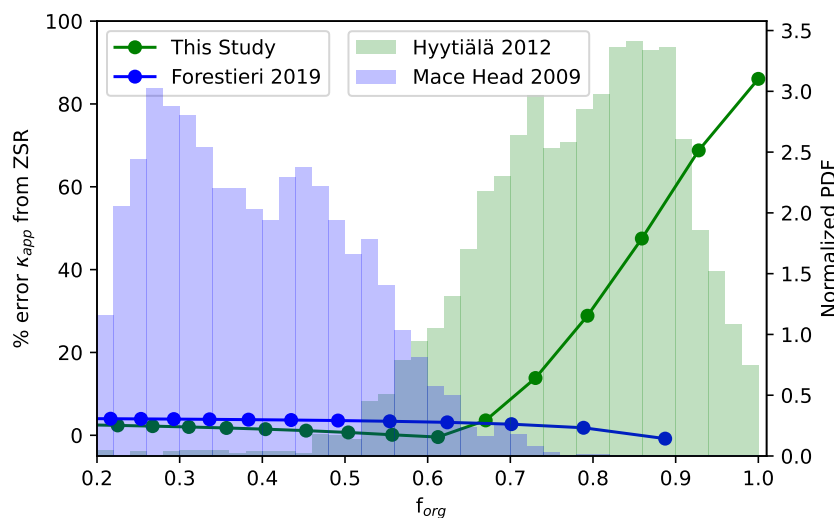
Figure 4.4: On the left axis, the percent error in κ_{app} for a mixed ammonium sulfate-organic aerosol calculated between a surface-active and non-surface-active organics case. The data for this study are for β-caryophyllene dark ozonolysis, and the data for Forestieri et al are for oleic acid. PDFs of Mace Head and Hyytiälä f_{org} data shown in the background (on the right axis).

organic ratios, we calculated the percent difference in the ZSR-estimated κ and the apparent κ with surface-active organics for two cases: the compressed film parameters of the β-caryophyllene dark ozonolysis in this work, and the oleic acid parameters from Forestieri and colleagues. These results are shown in Figure 4.4. Across the range of organic volume fractions considered, oleic acid shows no discernible differences in κ, while for β-caryophyllene SOA we observe more than 80% error in apparent κ at the highest volume fractions (f_{org}). Note that for oleic acid, at $f_{org} > 0.9$, the errors trend to 0. Interestingly, when we overlay the ambient data PDFs, we can see that where the most error in κ is observed is also well within the observed ambient species, suggesting that for boreal forest OA, there may be a substantial impact of surface-partitioning on the CCN population. This is not the case for the marine environment, where low ambient organic fractions are observed, and the impacts of surface partitioning on κ appear to be minimal.

As a final test of potential impacts, we performed an adiabatic parcel study. The parcel model is that described by Seinfeld and Pandis, and all other relevant parameters (e.g., size distribution, updraft velocity, organic volume fraction) are taken from Lowe et al. Table 1 for the Hyytiälä boreal forest case (Lowe et al., 2019; Schulze et al., 2020; Seinfeld & Pandis, 2016). We vary κ as such: for the base
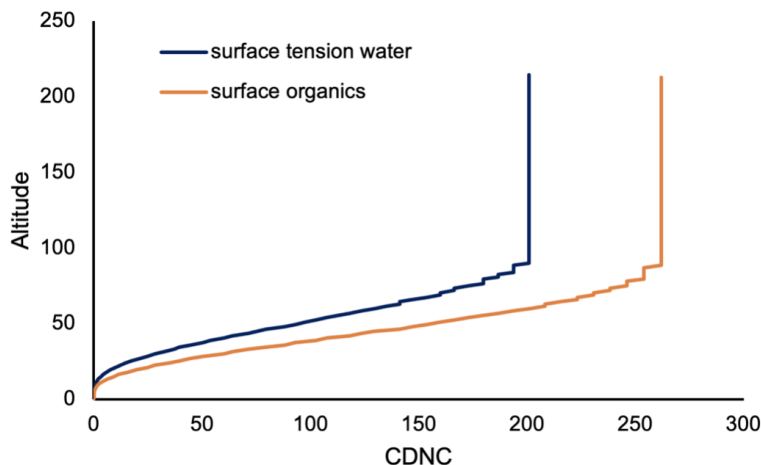
Figure 4.5: Cloud Droplet Number Concentration (CDNC) altitude profile. The two cases are for runs of Lowe et al. parameters in addition to this work's measured κ values for the β-caryophyllene dark ozonolysis case. The surface organics case employs the enhanced κ_{org} inferred from the lab studies in this work. The "surface tension water" case employs the intrinsic κ for the β-caryophyllene SOA (here measured as 0.02).

case ("surface tension water") we use κ = 0.02 for the organic fraction; for the surface-active organics case ("surface organics") we take the corresponding measured κ_{org} inferred by our data (see Figure 4.2). The parcel simulations are shown in Figure 4.5. Above cloud base, we can observe a 30% enhancement in CDNC in the surface-active case. Of note, the parameterized organic fraction is 0.67, which is a modest organic fraction by ambient standards (see Figure 4.4); therefore, we can expect this to be a lower limit impact on the CDNC. However, we acknowledge that this model is not a representation of the true scenario; here we have not had a dynamic activation process, rather just used the surface tension of water as opposed to a depressed surface tension. In future work, we will analyze the full impacts in a parcel-based model framework for better representativeness (De Jong et al., 2023).

Nonetheless, it is important to acknowledge that impacts to the cloud properties shown by this data do suggest potential implications for cloud formation processes, and are in line with other modeling studies (Lowe et al., 2019). However, it is also worth noting that, from a global modeling perspective, it is interesting that these parameters for sea spray mimics do not show significant implications for marine CCN. Marine clouds make up a substantially larger fraction of clouds than those impacted by boreal forests (just by surface area arguments alone), and so it does

raise the question of whether or not this level of detail is worth incorporating in model settings. Indeed, the key utility of the κ framework is not that it is a complete physciochemical descriptor of the aerosol, but in fact the opposite; its power lies in its simplicity.

4.5 Supporting Information

Compressed Film Framework Expanded

The framework used to describe the surface partitioning in this study, called here the compressed film model, has been presented elsewhere (Forestieri et al., 2018; Ruehl et al., 2016; Vepsäläinen et al., 2022). We re-describe its important features here for clarity. This model essentially allows for two particle phases: a bulk phase and a surface phase. For the purposes of this work, the surface phase is the SOA coating and the bulk phase is a ternary water-inorganic-organic solution. As water uptake occurs, the organic coating slowly decreases in diameter until a monolayer is achieved (i.e., a layer with thickness of one molecule), and finally a phase transition occurs at this two-dimensional interface where the surface phase becomes gaseous. Correspondingly over this growth, the particle surface tension is that of the organic coating at large thicknesses, and relaxes towards that of water as water is taken up. After the phase transition (or monolayer breakup), the surface tension is taken as that or water.

Mathematically, we are interested in describing how the concentration of the organic partitions between the two phases (surface and bulk) during water uptake. The organic concentration in the bulk phase is described as:

$$C_{bulk} = (1 - f_{surf}) \frac{(d_{coat}^3 - d_{seed}^3)\overline{v}_w}{d_{wet}^3 \overline{v}_{org}} \tag{4.4}$$

where f_{surf} is the concentration of organic molecules adsorbed to the surface, d_{seed} is the diameter of the ammonium sulfate seed aerosol, d_{coat} is the diameter of the SOA-coated particle, d_{wet} is the diameter of the droplet at some point during the activation process, $\overline{v}_w$ is the molar volume of water, and $\overline{v}_{org}$ is the molar volume of the SOA. Notice that this term (C_{bulk}) is non-dimensional and is the ratio of the moles of organic to moles of water in the bulk. The molar volume of the SOA is in this work assumed, as SOA is not a single species (which would correspond to a single molecular weight); see later discussion on molecular weight estimation. The amount of organic at the surface (A) is described not in terms of a concentration,

but rather the average surface area per adsorbed molecule:

$$A = \frac{6\bar{v}_{org}d_{wet}^2}{f_{surf}(d_{coat}^3 - d_{seed}^3)N_A} \tag{4.5}$$

where N_A is the Avogadro constant. While it may seem odd to use the adsorbed area instead of a concentration (which is the quantity we are effectively seeking to calculate), this description holds physically across the transition from a three dimensional coating through two dimensional phase change. Intuitively, a smaller adsorbed area per molecule (aka a smaller value of A), suggests a thicker coating of SOA (which scales inversely with d_{wet}, as we would expect).

To relate the surface and bulk concentrations, we use the isotherm of the equation of state, calculated as:

$$\ln\left(\frac{C_{bulk}}{C_0}\right) = (A_0^2 - A^2)\frac{m_\sigma N_A}{2RT} \tag{4.6}$$

where C_0 is the bulk concentration at which half the surface sites are occupied, A_0 is the critical molecular area (i.e. the area taken up by one molecule at the surface), m_σ parameterizes interactions between surfactants at the interface, R is the ideal gas constant, and T is the temperature. These surface parameters are in turn used to calculate the surface tension (σ), which is defined as:

$$\sigma = \min(\sigma_{min}, \sigma_w - (A_0 - A)m_\sigma) \tag{4.7}$$

where σ_{min} is the minimum surface tension and σ_w is the surface tension of water. In this work, σ_{min} is the surface tension of a pure SOA layer, which is assumed to be less than that of water. This has been shown for pinene and caryophyllene derivatives in bulk solution measurements (Gray Bé et al., 2017).

Importantly, this model allows us to dynamically calculate two terms: the surface tension and the water activity. So, we can reformulate our calculation of the saturation vapor pressure of our particle as:

$$S = \frac{n_w}{n_w + \phi_{inorg}n_{inor} + \phi_{org}n_{org}} \exp\left(\frac{4\sigma M_w}{RT\rho_w d_{wet}}\right) \tag{4.8}$$

where n_w, n_{inorg}, and n_{org} refer to the number of moles of water, inorganic, and organic present in the bulk solution, ϕ_{inorg} and ϕ_{org} are the the Vant Hoff factors for the inorganic and organic constituents, and σ is the surface tension calculated by equation (4.7). The first fraction on the RHS of equation (4.8) is the water

activity, which is calculated dynamically based on the amount of organics actually dissolved in the bulk vs the amount partitioned to the surface (recall this is modulated by the f_{surf} term in previous equations). This allows the generation of a Köhler curve with a saturation ratio calculated from the dynamic surface tension and water activity terms. Form this Köhler curve, we can extract an apparent hygroscopicity (κ_{app}), which is essentially the κ that corresponds to the critical supersaturation and activation diameter of an aerosol not undergoing surface partitioning. In general, because the critical supersaturation is lowered, the κ_{app} should be higher than what you expect for the pure species. These κ values (and all κ's in this work) are estimated through a gradient-descent algorithm solving Equation 6 in the work of Petters and Kreidenweis (Petters & Kreidenweis, 2007).
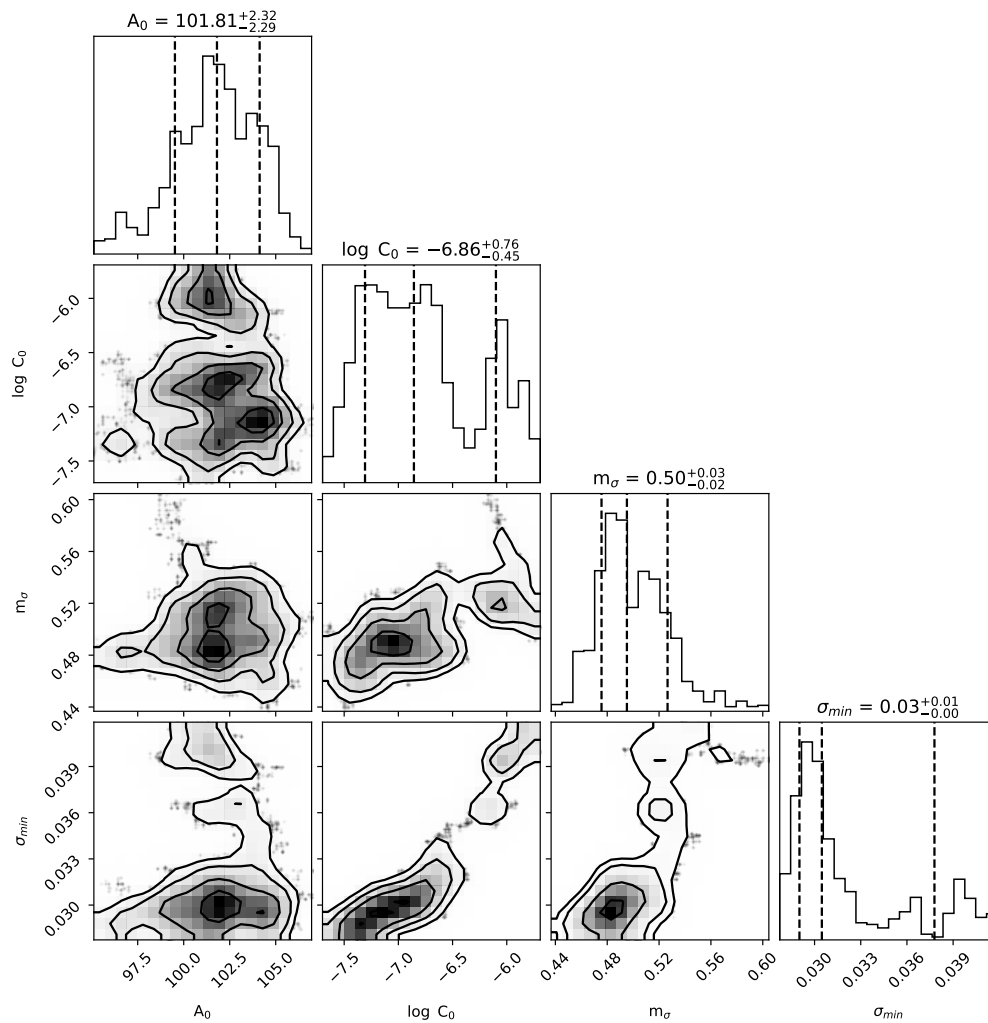
Figure 4.6: Corner plot for 4-parameter MCMC estimation for the β-caryophyllene dark ozonolysis data.

Figure 4.7: Corner plot for 4-parameter MCMC estimation for the β-caryophyllene photoxidation data.

Figure 4.8: Corner plot for 4-parameter MCMC estimation for the α-pinene dark ozonolysis data.

Figure 4.9: Corner plot for 4-parameter MCMC estimation for the α-pinene photoxidation data.
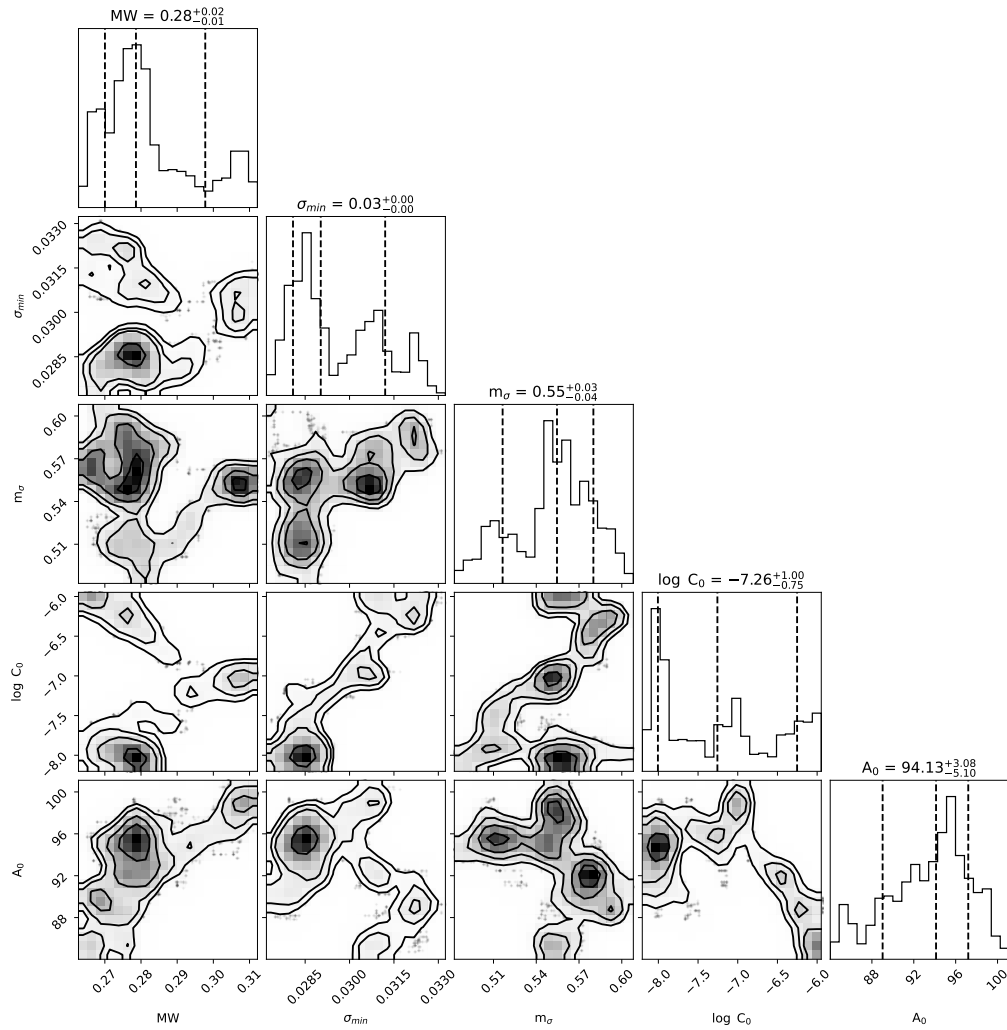
Figure 4.10: Corner plot for 5-parameter MCMC estimation for the β-caryophyllene dark ozonolysis data.
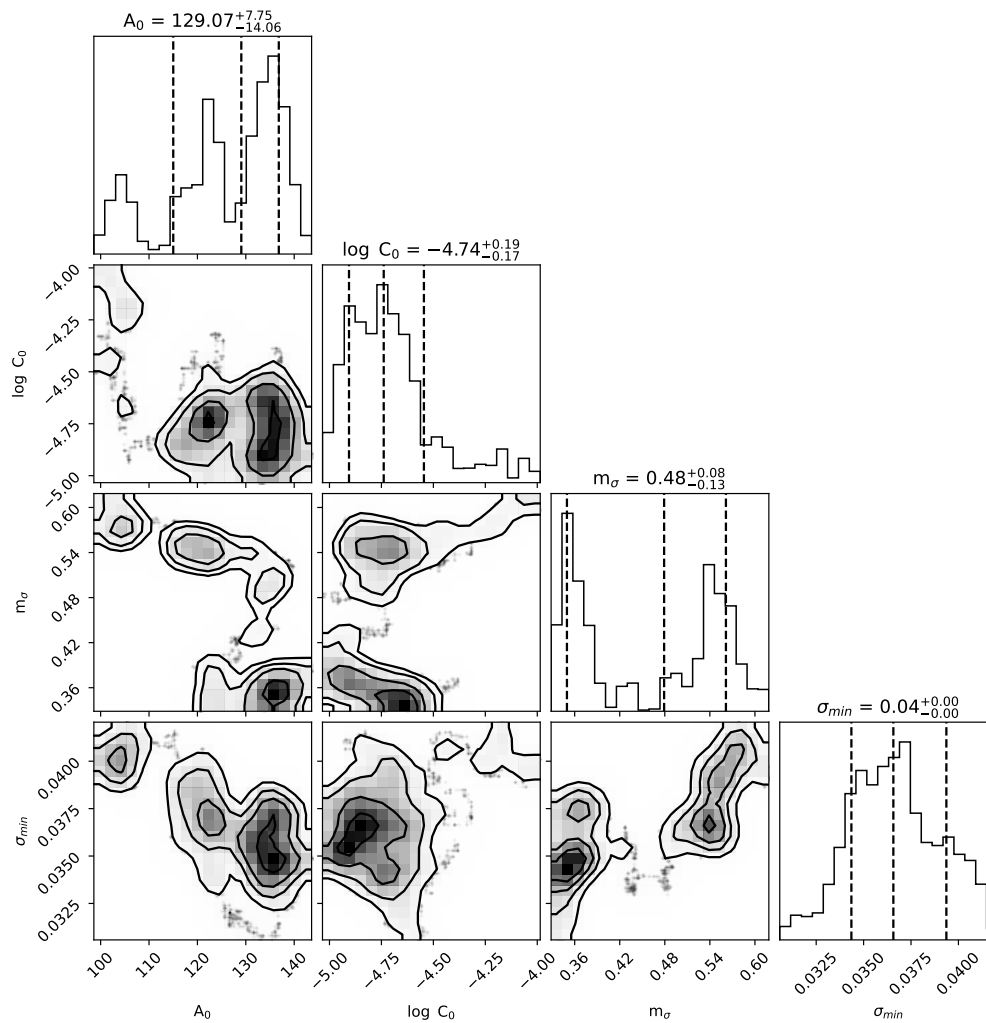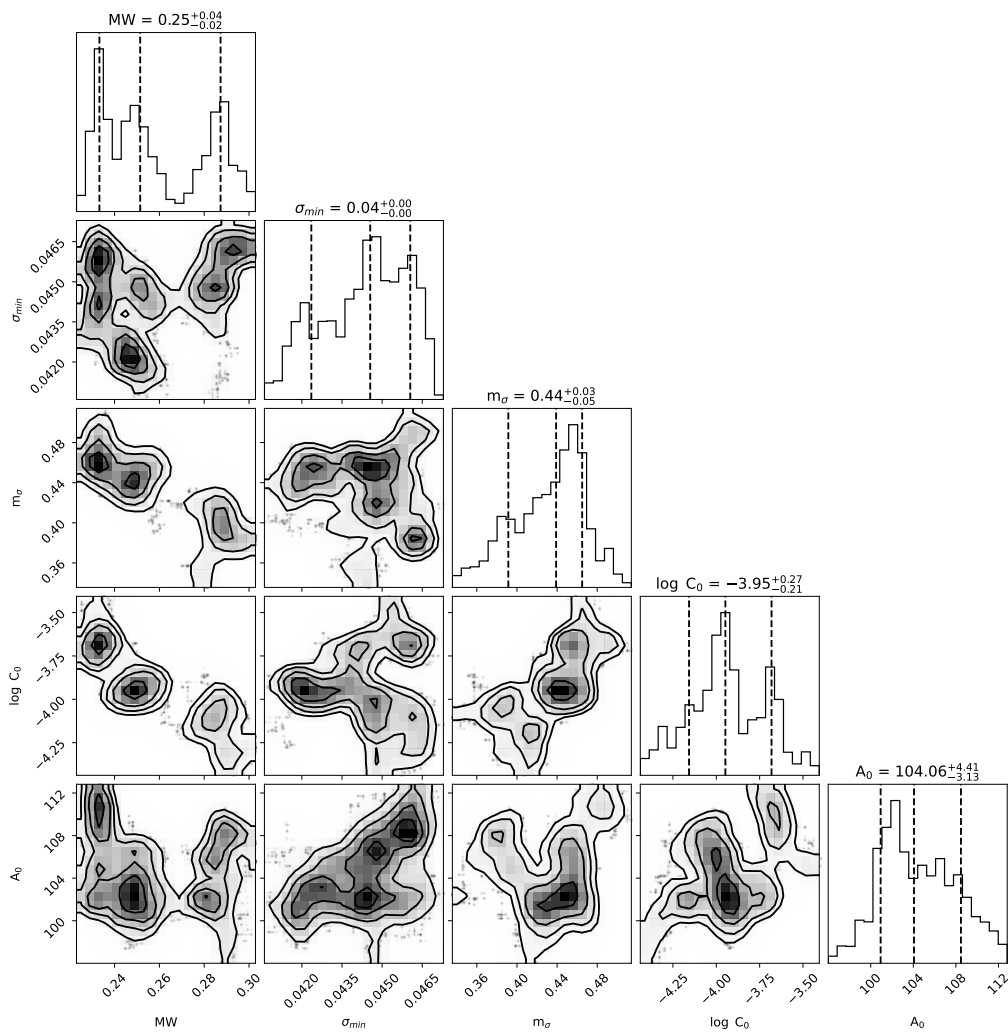
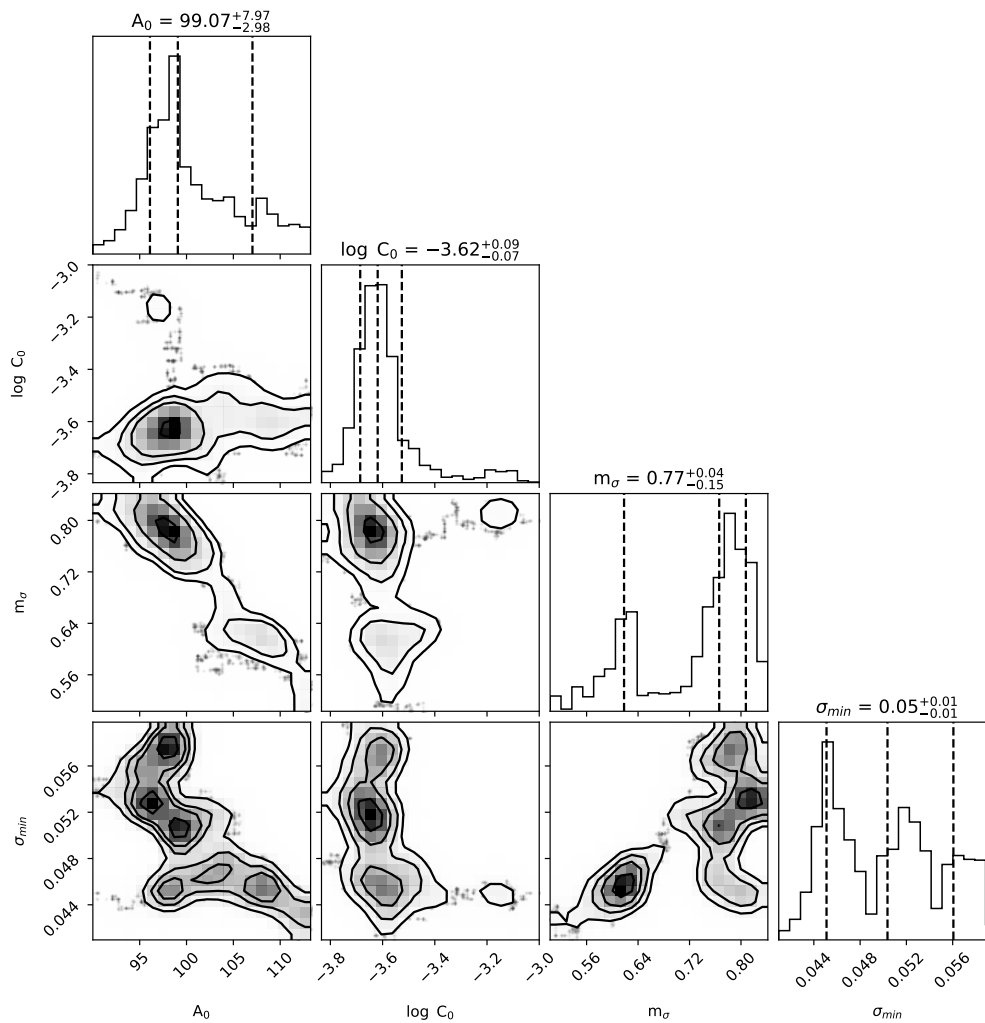Figure 4.11: Corner plot for 5-parameter MCMC estimation for the β-caryophyllene photoxidation data.
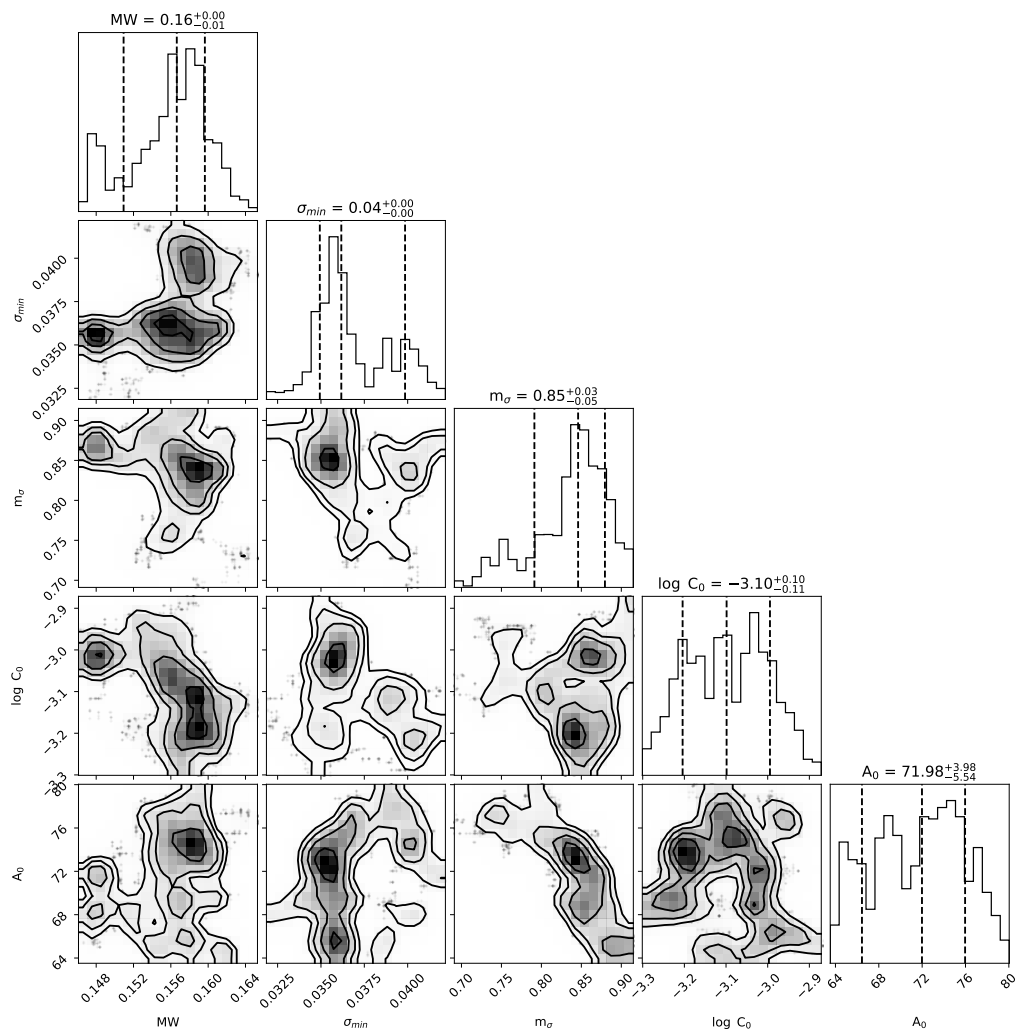
Figure 4.12: Corner plot for 5-parameter MCMC estimation for the α-pinene dark ozonolysis data.
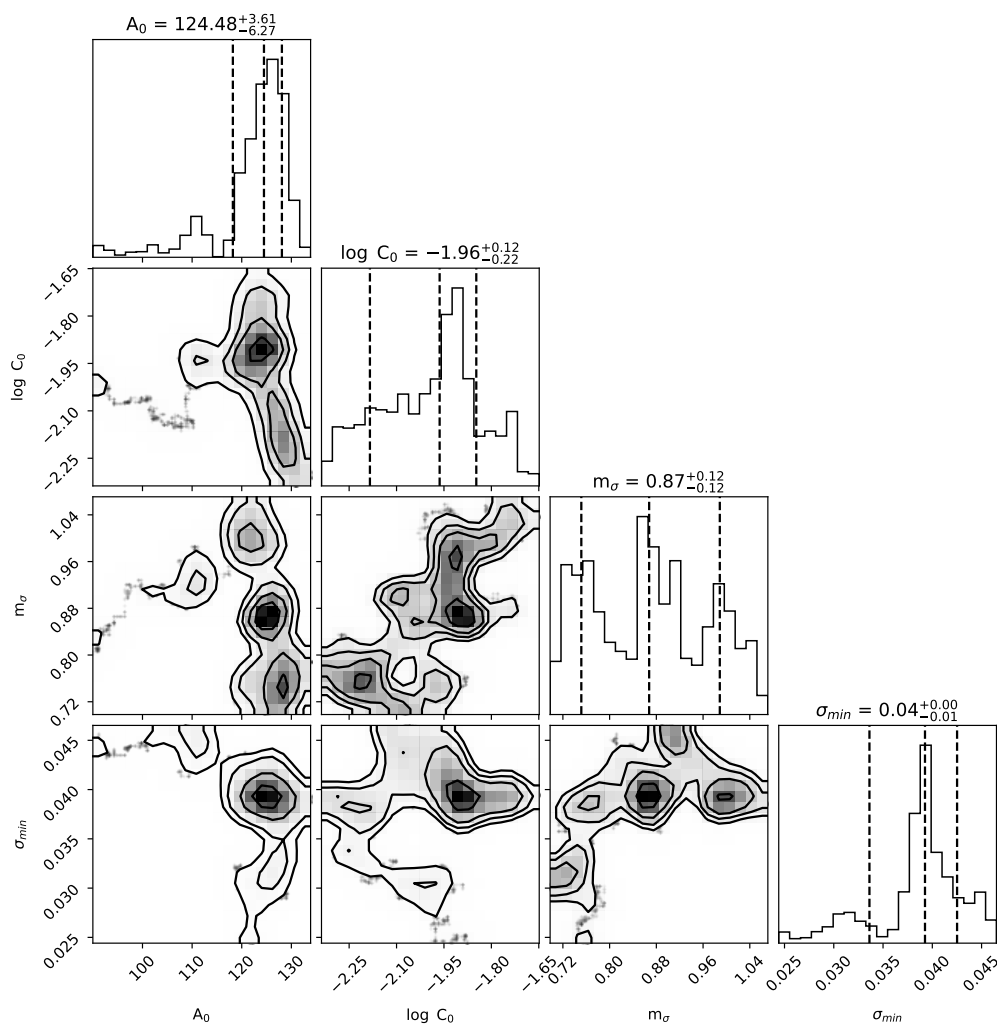
Figure 4.13: Corner plot for 5-parameter MCMC estimation for the α-pinene pho-toxidation data.

Figure 4.14: Corner plot for the iso-σ MCMC estimation for the β-caryophyllene dark ozonolysis data.

Figure 4.15: Corner plot for iso-σ MCMC estimation for the β-caryophyllene photoxidation data.

Figure 4.16: Corner plot for iso-σ MCMC estimation for the α-pinene dark ozonolysis data.

Figure 4.17: Corner plot for iso-σ MCMC estimation for the α-pinene photoxidation data.
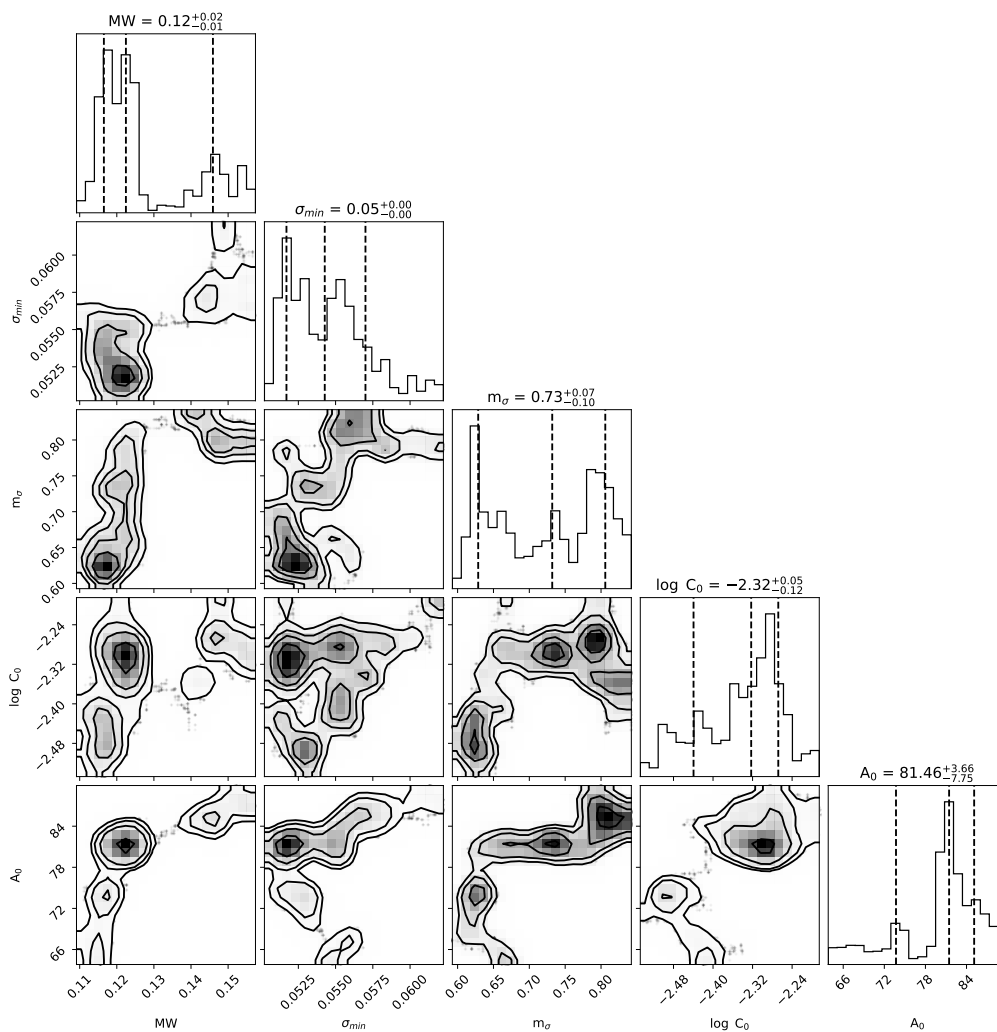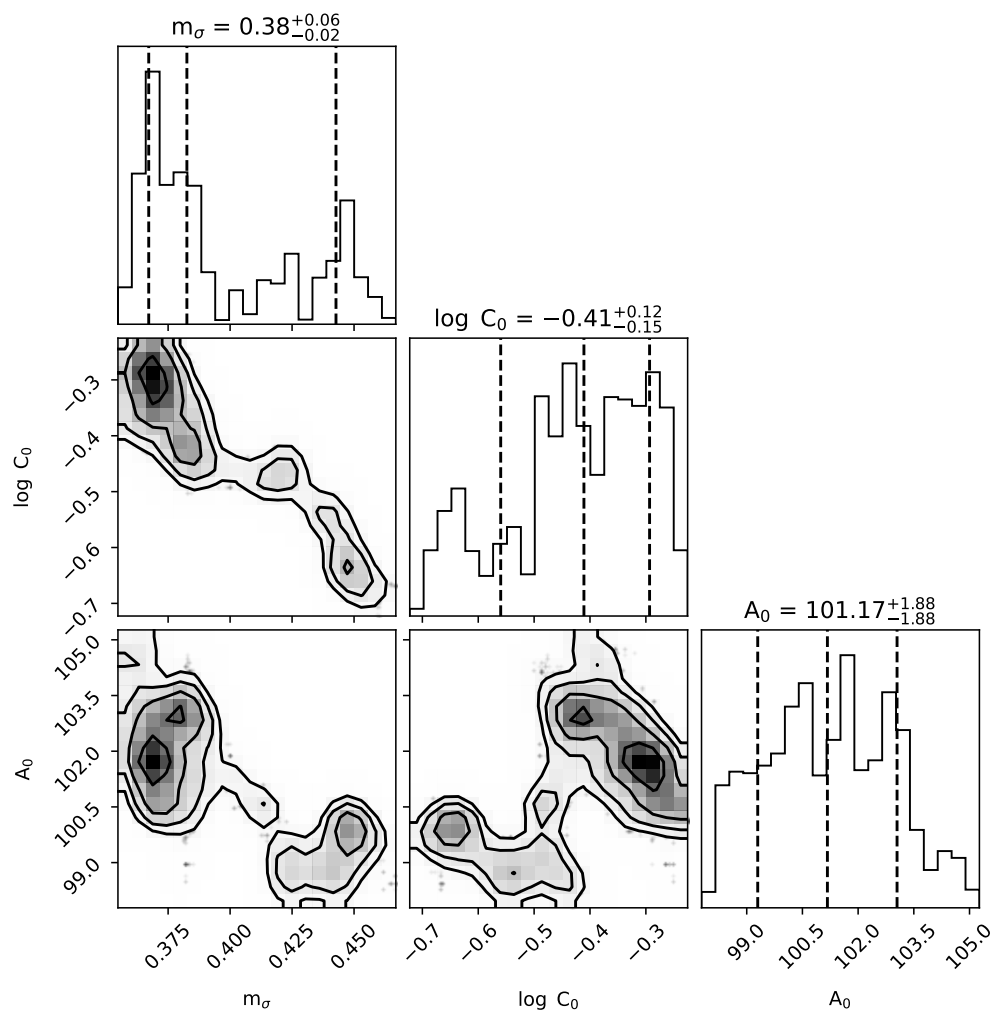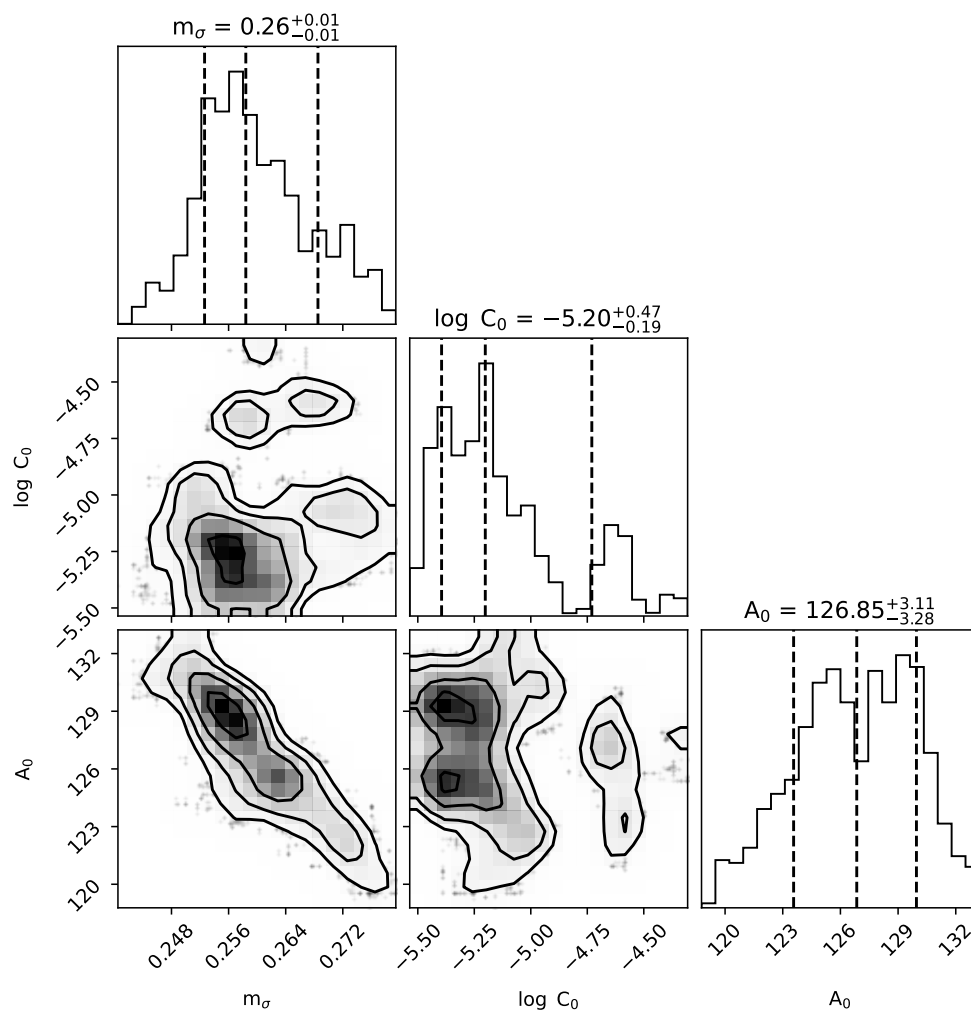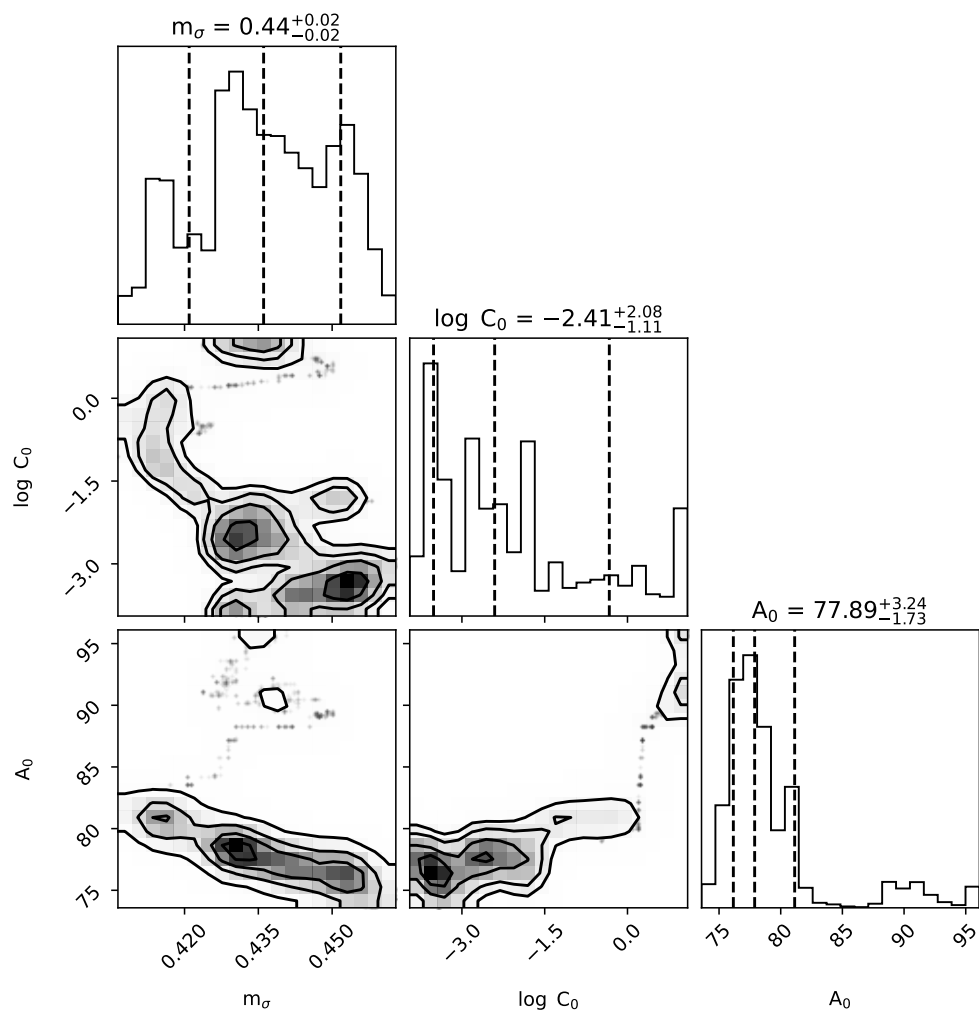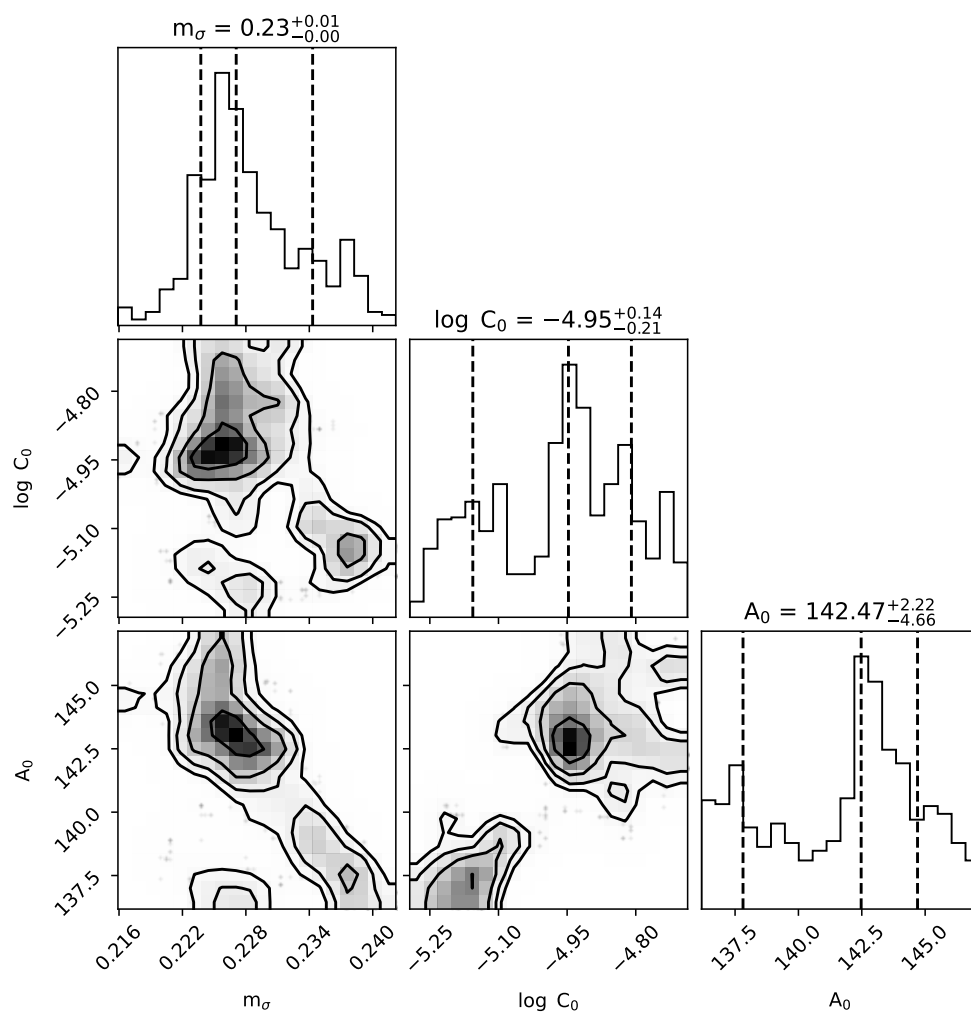
Molecular Weight Estimation

An understanding of the true molecular weight of SOA would require the knowledge of (1) the identity of every species present in the SOA, and (2) the relative abundances of those species. We are not privy to either of these. In general, the oxidation process adds oxygen(s) to a precursor VOC, and so the resulting species partitioning to the SOA are heavier than their parent compound. However, processes like fragmentation can also reduce the molecular weight of the resulting species. Again, we are not privy to the relative chemical pathways of the SOA generated in this work.

So, we generate a proxy for the molecular weight of SOA based on the chamber studies reported by Claffin et al., who measured the nominal molecular weight of SOA based on spectroscopic measurements of the relative amounts of functional groups present in α-pinene SOA (Claflin et al., 2018). From their data, we generate a crude parameterization:

$$MW = 153.33 \times O:C + 138.72 \qquad (4.9)$$

where MW is the molecular weight and O:C is reported by the AMS measurements. From our data, we identify the following four molecular weights: 298.6 g mol^{-1} for β-caryophyllene + O$_3$, 359.9 g mol^{-1} for β-caryophyllene + OH, 209.3 g mol^{-1} α-pinene + O$_3$, and 264.9 g mol^{-1} α-pinene + OH. In general, there is an assumption that oligermization is dominating fragmentation, so the molecular weight scales as O:C. While this parameterization is likely not a great representation of the SOA condition, it is only in service of data fits.

Mess Spectral Data

Presented in Figures 4.18 and 4.19 are AMS spectra from the representative cases. These are time-averaged, steady-state spectra generated in the flow tube, and their normalized values are shown to facilitate comparison. As one would expect, in the photoxidation cases, where the extent of oxidation is higher as measured by the oxygen-to-carbon ratio, there are enhancements at m/z 44, corresponding to CO$_2^+$. This is a bulk measurement of the aerosol population, though, and does not represent the changing chemical compositions which may exists across the size range of the SOA in this study (Tu & Johnston, 2017). In other words, each κ measurement reported in this study is from a monodisperse distribution, but the AMS measures everything generated in the flow tube (the monodisperse mass loading was often too small to reliably measure the elemental composition). For the scope of attributing chemical effects to CCN activity in this study, we explicitly assume that across the
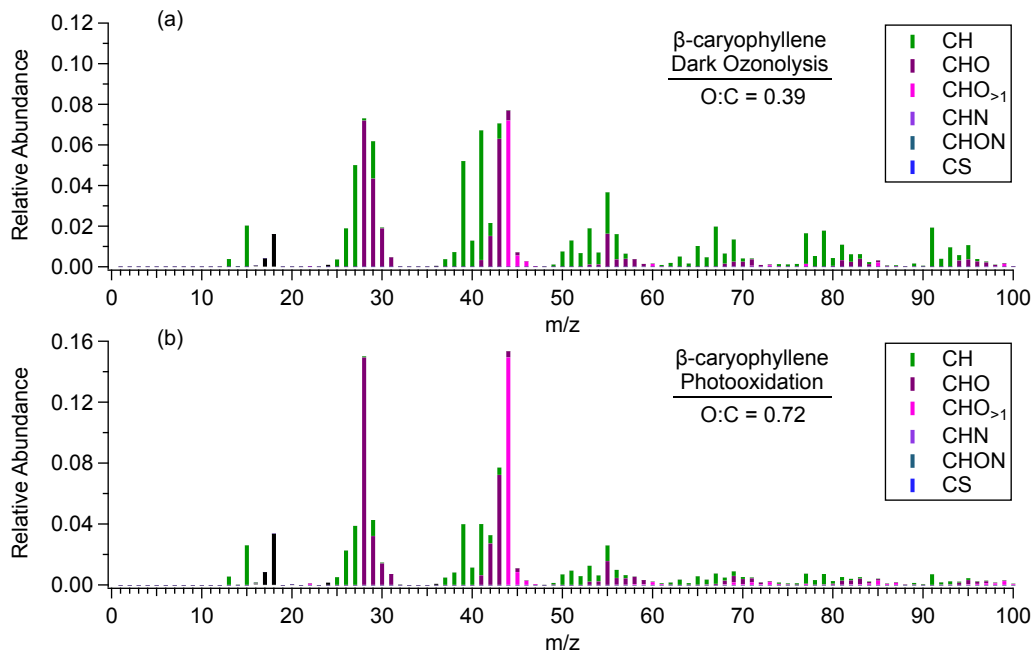
Figure 4.18: Representative AMS spectra for the β-caryophyllene experiments.

size range of importance (50 nm - 110 nm), processes such as fragmentation and oligomerization, which may alter the partitioning or particle-phase composition, are uniform to the extent that the surface-effects are uniform.

Experimental Set-up

Presented in Figure 4.20 is the experimental set-up. sVOCs, oxidants, and seed aerosol were injected at the inlet side (left of the schematic) of the flow tube (CPOT). The seed, ammonium sulfate, was size-selected in the range of 30 and 50 nm; so, a monodisperse distribution was always injected. The SOA resulting from the precursor VOC condensed onto the seed, which generated a polydisperse size-distribution inside of CPOT. The bulk properties of this process, including the size distribution and the chemical composition, were measured at the outlet by DMA and AMS. Another DMA was also used to select a monodisperse size at the outlet; thus with a known seed size and known classified coated size, the organic volume fraction was calculated.
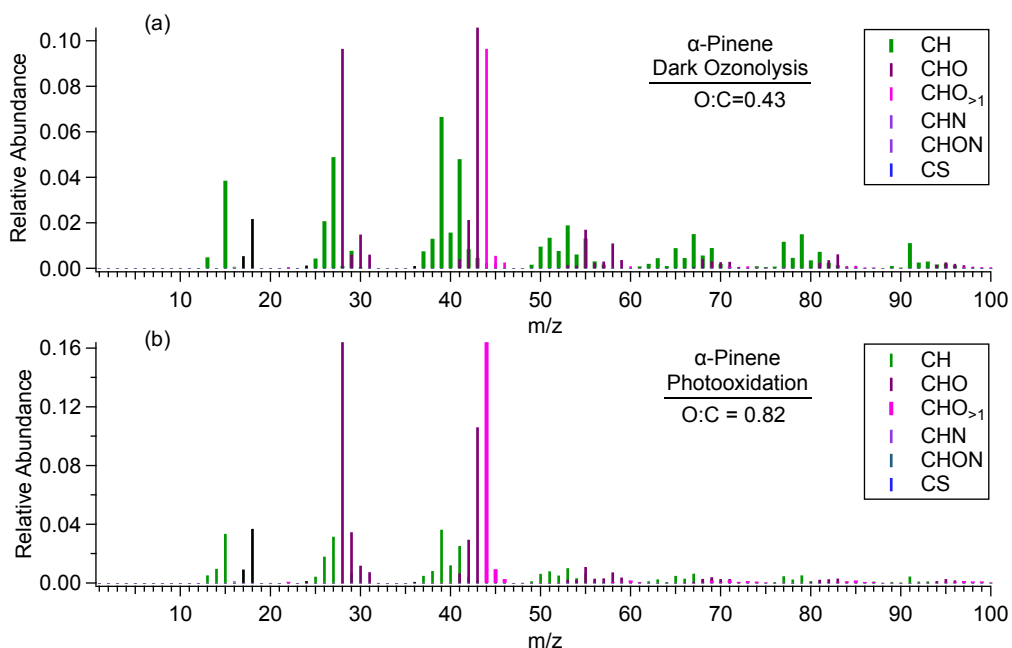
Figure 4.19: Representative AMS spectra for the α-pinene experiments.
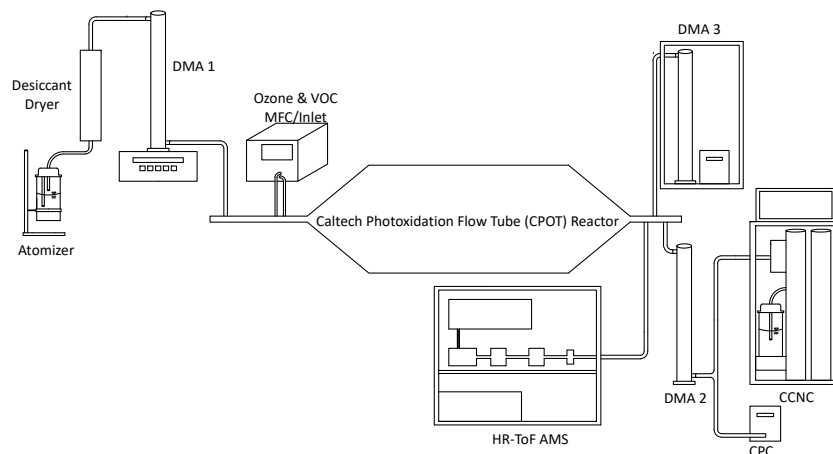
Figure 4.20: Experimental schematic. Monodisperse ammonium sulfate particles enter CPOT from DMA 1. SOA is generated in CPOT and condenses onto the seed, creating a polydisperse distribution. These particles are then size-selected by DMA 2, thus tuning the ratio of inorganic (seed) and organic (condensate). Bulk CPOT particle properties are measured by DMA 3 (size distribution) and the AMS (chemical composition).

References

Asa-Awuku, A., Engelhart, G. J., Lee, B. H., Pandis, S. N., & Nenes, A. (2009). Relating CCN activity, volatility, and droplet growth kinetics of -caryophyllene secondary organic aerosol. *Atmospheric Chemistry and Physics*, *9*(3), 795–812. https://doi.org/10.5194/acp-9-795-2009

Canagaratna, M. R., Jimenez, J. L., Kroll, J. H., Chen, Q., Kessler, S. H., Massoli, P., Hildebrandt Ruiz, L., Fortner, E., Williams, L. R., Wilson, K. R., Surratt, J. D., Donahue, N. M., Jayne, J. T., & Worsnop, D. R. (2015). Elemental ratio measurements of organic compounds using aerosol mass spectrometry: Characterization, improved calibration, and implications. *Atmospheric Chemistry and Physics*, *15*(1), 253–272. https://doi.org/10.5194/acp-15-253-2015

Claflin, M. S., Krechmer, J. E., Hu, W., Jimenez, J. L., & Ziemann, P. J. (2018). Functional Group Composition of Secondary Organic Aerosol Formed from Ozonolysis of -Pinene Under High VOC and Autoxidation Conditions. *ACS Earth and Space Chemistry*, *2*(11), 1196–1210. https://doi.org/10.1021/acsearthspacechem.8b00117

Dall'Osto, M., Ceburnis, D., Martucci, G., Bialek, J., Dupuy, R., Jennings, S. G., Berresheim, H., Wenger, J., Healy, R., Facchini, M. C., Rinaldi, M., Giulianelli, L., Finessi, E., Worsnop, D., Ehn, M., Mikkilä, J., Kulmala, M., & O'Dowd, C. D. (2010). Aerosol properties associated with air masses arriving into the North East Atlantic during the 2008 Mace Head EUCAARI intensive observing period: An overview. *Atmospheric Chemistry and Physics*, *10*(17), 8413–8435. https://doi.org/10.5194/acp-10-8413-2010

Davies, J. F., Zuend, A., & Wilson, K. R. (2018). Technical Note: The Role of Evolving Surface Tension in the Formation of Cloud Droplets. *Atmospheric Chemistry and Physics Discussions*, 1–30. https://doi.org/10.5194/acp-2018-1201

De Jong, E. K., Singer, C. E., Azimi, S., Bartman, P., Bulenok, O., Derlatka, K., Dula, I., Jaruga, A., Mackay, J. B., Ward, R. X., & Arabas, S. (2023). New developments in PySDM and PySDM-examples v2:collisional breakup, immersion freezing, dry aerosol initialization, andadaptive time-stepping. *Journal of Open Source Software*, *8*(84), 4968. https://doi.org/10.21105/joss.04968

DeCarlo, P. F., Kimmel, J. R., Trimborn, A., Northway, M. J., Jayne, J. T., Aiken, A. C., Gonin, M., Fuhrer, K., Horvath, T., Docherty, K. S., Worsnop, D. R., & Jimenez, J. L. (2006). Field-Deployable, High-Resolution, Time-of-Flight Aerosol Mass Spectrometer. *Analytical Chemistry*, *78*(24), 8281–8289. https://doi.org/10.1021/ac061249n

Farmer, D. K., Cappa, C. D., & Kreidenweis, S. M. (2015). Atmospheric Processes and Their Controlling Influence on Cloud Condensation Nuclei Activity. *Chemical Reviews*, *115*(10), 4199–4217. https://doi.org/10.1021/cr5006292

Forestieri, S. D., Staudt, S. M., Kuborn, T. M., Faber, K., Ruehl, C. R., Bertram, T. H., & Cappa, C. D. (2018). Establishing the impact of model surfactants on cloud condensation nuclei activity of sea spray aerosol mimics. *Atmospheric Chemistry and Physics*, *18*(15), 10985–11005. https://doi.org/10.5194/acp-18-10985-2018

Frosch, M., Bilde, M., Nenes, A., Praplan, A. P., Jurányi, Z., Dommen, J., Gysel, M., Weingartner, E., & Baltensperger, U. (2013). CCN activity and volatility of -caryophyllene secondary organic aerosol [ISBN: 1322832013]. *Atmospheric Chemistry and Physics*, *13*(4), 2283–2297. https://doi.org/10.5194/acp-13-2283-2013

Gray Bé, A., Upshur, M. A., Liu, P., Martin, S. T., Geiger, F. M., & Thomson, R. J. (2017). Cloud Activation Potentials for Atmospheric -Pinene and -Caryophyllene Ozonolysis Products. *ACS Central Science*, *3*(7), 715–725. https://doi.org/10.1021/acscentsci.7b00112

Hakola, H., Hellén, H., Hemmilä, M., Rinne, J., & Kulmala, M. (2012). In situ measurements of volatile organic compounds in a boreal forest [Publisher: Copernicus GmbH]. *Atmospheric Chemistry and Physics*, *12*(23), 11665–11678. https://doi.org/10.5194/acp-12-11665-2012

Hakola, H., Tarvainen, V., Bäck, J., Ranta, H., Bonn, B., Rinne, J., & Kulmala, M. (2006). Seasonal variation of mono- and sesquiterpene emission rates of Scots pine [Publisher: Copernicus GmbH]. *Biogeosciences*, *3*(1), 93–101. https://doi.org/10.5194/bg-3-93-2006

Heikkinen, L., Äijälä, M., Daellenbach, K. R., Chen, G., Garmash, O., Aliaga, D., Graeffe, F., Räty, M., Luoma, K., Aalto, P., Kulmala, M., Petäjä, T., Worsnop, D., & Ehn, M. (2021). Eight years of sub-micrometre organic aerosol composition data from the boreal forest characterized using a machine-learning approach. *Atmospheric Chemistry and Physics*, *21*(13), 10081–10109. https://doi.org/10.5194/acp-21-10081-2021

Heikkinen, L., Äijälä, M., Riva, M., Luoma, K., Dällenbach, K., Aalto, J., Aalto, P., Aliaga, D., Aurela, M., Keskinen, H., Makkonen, U., Rantala, P., Kulmala, M., Petäjä, T., Worsnop, D., & Ehn, M. (2020). Long-term sub-micrometer aerosol chemical composition in the boreal forest: Inter- and intra-annual variability. *Atmospheric Chemistry and Physics*, *20*(5), 3151–3180. https://doi.org/10.5194/acp-20-3151-2020

Hu, W., Campuzano-Jost, P., Day, D. A., Nault, B. A., Park, T., Lee, T., Pajunoja, A., Virtanen, A., Croteau, P., Canagaratna, M. R., Jayne, J. T., Worsnop, D. R., & Jimenez, J. L. (2020). Ambient Quantification and Size Distributions for Organic Aerosol in Aerosol Mass Spectrometers with the New Capture

Vaporizer. *ACS Earth and Space Chemistry*, *4*(5), 676–689. https://doi.org/10.1021/acsearthspacechem.9b00310

Huang, Y., Coggon, M. M., Zhao, R., Lignell, H., Bauer, M. U., Flagan, R. C., & Seinfeld, J. H. (2017). The Caltech Photooxidation Flow Tube reactor: Design, fluid dynamics and characterization. *Atmospheric Measurement Techniques*, *10*(3), 839–867. https://doi.org/10.5194/amt-10-839-2017

Jayne, J. T., Leard, D. C., Zhang, X., Davidovits, P., Smith, K. A., Kolb, C. E., & Worsnop, D. R. (2000). Development of an Aerosol Mass Spectrometer for Size and Composition Analysis of Submicron Particles. *Aerosol Science and Technology*, *33*(1-2), 49–70. https://doi.org/10.1080/027868200410840

Kuwata, M., Zorn, S. R., & Martin, S. T. (2012). Using Elemental Ratios to Predict the Density of Organic Material Composed of Carbon, Hydrogen, and Oxygen. *Environmental Science & Technology*, *46*(2), 787–794. https://doi.org/10.1021/es202525q

Lance, S., Nenes, A., Medina, J., & Smith, J. N. (2006). Mapping the Operation of the DMT Continuous Flow CCN Counter. *Aerosol Science and Technology*, *40*(4), 242–254. https://doi.org/10.1080/02786820500543290

Lei, Z., Olson, N. E., Zhang, Y., Chen, Y., Lambe, A. T., Zhang, J., White, N. J., Atkin, J. M., Banaszak Holl, M. M., Zhang, Z., Gold, A., Surratt, J. D., & Ault, A. P. (2022). Morphology and Viscosity Changes after Reactive Uptake of Isoprene Epoxydiols in Submicrometer Phase Separated Particles with Secondary Organic Aerosol Formed from Different Volatile Organic Compounds. *ACS Earth and Space Chemistry*, *6*(4), 871–882. https://doi.org/10.1021/acsearthspacechem.1c00156

Li, W., Teng, X., Chen, X., Liu, L., Xu, L., Zhang, J., Wang, Y., Zhang, Y., & Shi, Z. (2021). Organic Coating Reduces Hygroscopic Growth of Phase-Separated Aerosol Particles. *Environmental Science & Technology*, *55*(24), 16339–16346. https://doi.org/10.1021/acs.est.1c05901

Lowe, S. J., Partridge, D. G., Davies, J. F., Wilson, K. R., Topping, D., & Riipinen, I. (2019). Key drivers of cloud response to surface-active organics [Publisher: Springer US]. *Nature Communications*, *10*(1). https://doi.org/10.1038/s41467-019-12982-0

Olson, N. E., Lei, Z., Craig, R. L., Zhang, Y., Chen, Y., Lambe, A. T., Zhang, Z., Gold, A., Surratt, J. D., & Ault, A. P. (2019). Reactive Uptake of Isoprene Epoxydiols Increases the Viscosity of the Core of Phase-Separated Aerosol Particles. *ACS Earth and Space Chemistry*, *3*(8), 1402–1414. https://doi.org/10.1021/acsearthspacechem.9b00138

Ovadnevaite, J., Zuend, A., Laaksonen, A., Sanchez, K. J., Roberts, G., Ceburnis, D., Decesari, S., Rinaldi, M., Hodas, N., Facchini, M. C., Seinfeld, J. H., & O'Dowd, C. (2017). Surface tension prevails over solute effect in organic-

influenced cloud droplet activation [Publisher: Nature Publishing Group]. *Nature*, *546*(7660), 637–641. https://doi.org/10.1038/nature22806

Pathak, R. K., Stanier, C. O., Donahue, N. M., & Pandis, S. N. (2007). Ozonolysis of -pinene at atmospherically relevant concentrations: Temperature dependence of aerosol mass fractions (yields) [_eprint: https://onlinelibrary.wiley.com/doi/pdf/10.1029/2006JD0 *Journal of Geophysical Research: Atmospheres*, *112*(D3). https://doi.org/ 10.1029/2006JD007436

Petäjä, T., Tabakova, K., Manninen, A., Ezhova, E., O'Connor, E., Moisseev, D., Sinclair, V. A., Backman, J., Levula, J., Luoma, K., Virkkula, A., Paramonov, M., Räty, M., Äijälä, M., Heikkinen, L., Ehn, M., Sipilä, M., Yli-Juuti, T., Virtanen, A., ... Kerminen, V.-M. (2022). Influence of biogenic emissions from boreal forests on aerosol–cloud interactions. *Nature Geoscience*, *15*(1), 42–47. https://doi.org/10.1038/s41561-021-00876-0

Petters, M. D., & Kreidenweis, S. M. (2007). A single parameter representation of hygroscopic growth and cloud condensation nucleus activity. *Atmospheric Chemistry and Physics*, *13*(2), 1961–1971. https://doi.org/10.5194/acp-13-1081-2013

Roberts, G. C., & Nenes, A. (2005). A Continuous-Flow Streamwise Thermal-Gradient CCN Chamber for Atmospheric Measurements. *Aerosol Science and Technology*, *39*(3), 206–221. https://doi.org/10.1080/027868290913988

Rose, D., Gunthe, S. S., Mikhailov, E., Frank, G. P., Dusek, U., Andreae, M. O., & Pöschl, U. (2008). Calibration and measurement uncertainties of a continuous-flow cloud condensation nuclei counter (DMT-CCNC): CCN activation of ammonium sulfate and sodium chloride aerosol particles in theory and experiment. *Atmospheric Chemistry and Physics*, *8*(5), 1153–1179. https://doi.org/10.5194/acp-8-1153-2008

Ruehl, C. R., Davies, J. F., & Wilson, K. R. (2016). An interfacial mechanism for cloud droplet formation on organic aerosols [ISBN: 10.1126/science.aad4889]. *Science*, *351*(6280), 1447–1450. https://doi.org/10.1126/science.aad4889

Ruehl, C. R., & Wilson, K. R. (2014). Surface organic monolayers control the hygroscopic growth of submicrometer particles at high relative humidity. *Journal of Physical Chemistry A*, *118*(22), 3952–3966. https://doi.org/10.1021/jp502844g

Salameh, A., Vorka, F., & Daskalakis, V. (2016). Correlation between Surface Tension and the Bulk Dynamics in Salty Atmospheric Aquatic Droplets. *The Journal of Physical Chemistry C*, *120*(21), 11508–11518. https://doi.org/10.1021/acs.jpcc.6b01842

Sareen, N., Schwier, A. N., Lathem, T. L., Nenes, A., & McNeill, V. F. (2013). Surfactants from the gas phase may promote cloud droplet formation. *Proceedings of the National Academy of Sciences*, *110*(8), 2723–2728. https://doi.org/10.1073/pnas.1204838110

Sareen, N., Waxman, E. M., Turpin, B. J., Volkamer, R., & Carlton, A. G. (2017). Potential of Aerosol Liquid Water to Facilitate Organic Aerosol Formation: Assessing Knowledge Gaps about Precursors and Partitioning. *Environmental Science & Technology*, *51*(6), 3327–3335. https://doi.org/10.1021/acs.est.6b04540

Schulze, B. C., Charan, S. M., Kenseth, C. M., Kong, W., Bates, K. H., Williams, W., Metcalf, A. R., Jonsson, H. H., Woods, R., Sorooshian, A., Flagan, R. C., & Seinfeld, J. H. (2020). Characterization of Aerosol Hygroscopicity Over the Northeast Pacific Ocean: Impacts on Prediction of CCN and Stratocumulus Cloud Droplet Number Concentrations [_eprint: https://onlinelibrary.wiley.com/doi/pdf/10.1029/20 *Earth and Space Science*, *7*(7), e2020EA001098. https://doi.org/10.1029/2020EA001098

Seinfeld, J. H., & Pandis, S. N. (2016). *Atmospheric Chemistry and Physics: From Air Pollution to Climate Change*. Wiley & Sons.

Shiraiwa, M., Zuend, A., Bertram, A. K., & Seinfeld, J. H. (2013). Gas–particle partitioning of atmospheric aerosols: Interplay of physical state, non-ideal mixing and morphology. *Physical Chemistry Chemical Physics*, *15*(27), 11441. https://doi.org/10.1039/c3cp51595h

Tasoglou, A., & Pandis, S. N. (2015). Formation and chemical aging of secondary organic aerosol during the -caryophyllene oxidation [Publisher: Copernicus GmbH]. *Atmospheric Chemistry and Physics*, *15*(11), 6035–6046. https://doi.org/10.5194/acp-15-6035-2015

Tu, P., & Johnston, M. V. (2017). Particle size dependence of biogenic secondary organic aerosol molecular composition. *Atmospheric Chemistry and Physics*, *17*(12), 7593–7603. https://doi.org/10.5194/acp-17-7593-2017

Twomey, S. (1974). Pollution and the planetary albedo. *Atmospheric Environment (1967)*, *8*(12), 1251–1256. https://doi.org/https://doi.org/10.1016/0004-6981(74)90004-3

Vepsäläinen, S., Calderón, S. M., Malila, J., & Prisle, N. L. (2022). Comparison of six approaches to predicting droplet activation of surface active aerosol – Part 1: Moderately surface active organics. *Atmospheric Chemistry and Physics*, *22*(4), 2669–2687. https://doi.org/10.5194/acp-22-2669-2022

Wang, J., Shilling, J. E., Liu, J., Zelenyuk, A., Bell, D. M., Petters, M. D., Thalman, R., Mei, F., Zaveri, R. A., & Zheng, G. (2019). Cloud droplet activation of secondary organic aerosol is mainly controlled by molecular weight, not water solubility. *Atmospheric Chemistry and Physics*, *19*(2), 941–954. https://doi.org/10.5194/acp-19-941-2019

Winterhalter, R., Herrmann, F., Kanawati, B., Nguyen, T. L., Peeters, J., Vereecken, L., & Moortgat, G. K. (2009). The gas-phase ozonolysis of -caryophyllene (C15H 24). Part I: An experimental study. *Physical Chemistry Chemical Physics*, *11*(21), 4152–4172. https://doi.org/10.1039/b817824k

Yli-Juuti, T., Mielonen, T., Heikkinen, L., Arola, A., Ehn, M., Isokääntä, S., Keski-nen, H.-M., Kulmala, M., Laakso, A., Lipponen, A., Luoma, K., Mikkonen, S., Nieminen, T., Paasonen, P., Petäjä, T., Romakkaniemi, S., Tonttila, J., Kokkola, H., & Virtanen, A. (2021). Significance of the organic aerosol driven climate feedback in the boreal area. *Nature Communications*, *12*(1), 5637. https://doi.org/10.1038/s41467-021-25850-7

METHANE EMISSIONS FROM DAIRY OPERATIONS IN CALIFORNIA'S SAN JOAQUIN VALLEY EVALUATED USING AIRBORNE FLUX MEASUREMENTS

Schulze, B. C., Ward, R. X., Pfannerstill, E. Y., Zhu, Q., Arata, C., Place, B., Nussbaumer, C., Wooldridge, P., Woods, R., Bucholtz, A., Cohen, R. C., Goldstein, A. H., Wennberg, P. O., & Seinfeld, J. H. (2023). Methane Emissions from Dairy Operations in California's San Joaquin Valley Evaluated Using Airborne Flux Measurements. *Environmental Science & Technology*, *57*(48), 19519–19531. https://doi.org/10.1021/acs.est.3c03940

Appendix B

TEMPERATURE-DEPENDENT EMISSIONS DOMINATE AEROSOL AND OZONE FORMATION IN LOS ANGELES

Pfannerstill, E. Y., Arata, C., Zhu, Q., Schulze, B. C., Ward, R., Woods, R., Harkins, C., Schwantes, R. H., Seinfeld, J. H., Bucholtz, A., Cohen, R. C., & Goldstein, A. H. (2024). Temperature-dependent emissions dominate aerosol and ozone formation in Los Angeles. *Science*, *384*(6702), 1324–1329. https://doi.org/10.1126/science. adg8204

A p p e n d i x   C

ASSESSING THE INFLUENCE OF COVID-19 ON THE SHORTWAVE RADIATIVE FLUXES OVER THE EAST ASIAN MARGINAL SEAS

Ming, Y., Loeb, N. G., Lin, P., Shen, Z., Naik, V., Singer, C. E., Ward, R. X., Paulot, F., Zhang, Z., Bellouin, N., Horowitz, L. W., Ginoux, P. A., & Ramaswamy, V. (2020). Assessing the influence of COVID-19 on the shortwave radiative fluxes over the East Asian Marginal Seas. *Geophysical Research Letters*. https://doi.org/10.1029/2020gl091699

Appendix D

QUANTIFICATION OF FACE SEAL LEAKAGE USING PARALLEL RESISTANCE MODEL

Pushpawela, B., Chea, P., Ward, R., & Flagan, R. C. (2023). Quantification of face seal leakage using parallel resistance model. *Physics of Fluids*, *35*(12), 127127. https://doi.org/10.1063/5.0177717

A p p e n d i x   E

IS DOUBLE MASKING EVEN WORTHWHILE?

Chea, P. H., Pushpawela, B., Ward, R. X., & Flagan, R. C. (2024). Is double masking even worthwhile? *Aerosol Science and Technology*, 1–13. https://doi.org/10.1080/02786826.2024.2369638

Appendix F

MEASUREMENT REPORT: AIRBORNE MEASUREMENTS OF NO$_x$ FLUXES OVER LOS ANGELES DURING THE RECAP-CA 2021 CAMPAIGN

Nussbaumer, C. M., Place, B. K., Zhu, Q., Pfannerstill, E. Y., Wooldridge, P., Schulze, B. C., Arata, C., Ward, R., Bucholtz, A., Seinfeld, J. H., Goldstein, A. H., & Cohen, R. C. (2023). Measurement report: Airborne measurements of NO$_x$ fluxes over Los Angeles during the RECAP-CA 2021 campaign. *Atmospheric Chemistry and Physics*, *23*(20), 13015–13028. https://doi.org/10.5194/acp-23-13015-2023

AN UPDATED MODELING FRAMEWORK TO SIMULATE LOS ANGELES AIR QUALITY – PART 1: MODEL DEVELOPMENT, EVALUATION, AND SOURCE APPORTIONMENT

Pennington, E. A., Wang, Y., Schulze, B. C., Seltzer, K. M., Yang, J., Zhao, B., Jiang, Z., Shi, H., Venecek, M., Chau, D., Murphy, B. N., Kenseth, C. M., Ward, R. X., Pye, H. O. T., & Seinfeld, J. H. (2024). An updated modeling framework to simulate Los Angeles air quality – Part 1: Model development, evaluation, and source apportionment. *Atmospheric Chemistry and Physics*, *24*(4), 2345–2363. https://doi.org/10.5194/acp-24-2345-2024

A p p e n d i x   H

EFFICACY OF A PORTABLE, MODERATE-RESOLUTION, FAST-SCANNING DIFFERENTIAL MOBILITY ANALYZER FOR AMBIENT AEROSOL SIZE DISTRIBUTION MEASUREMENTS

Amanatidis, S., Huang, Y., Pushpawela, B., Schulze, B. C., Kenseth, C. M., Ward, R. X., Seinfeld, J. H., Hering, S. V., & Flagan, R. C. (2021). Efficacy of a portable, moderate-resolution, fast-scanning differential mobility analyzer for ambient aerosol size distribution measurements. *Atmospheric Measurement Techniques*, *14*(6), 4507–4516. https://doi.org/10.5194/amt-14-4507-2021

Appendix I

NEW DEVELOPMENTS IN PYSDM AND PYSDM-EXAMPLES V2: COLLISIONAL BREAKUP, IMMERSION FREEZING, DRY AEROSOL INITIALIZATION, AND ADAPTIVE TIME-STEPPING

De Jong, E. K., Singer, C. E., Azimi, S., Bartman, P., Bulenok, O., Derlatka, K., Dula, I., Jaruga, A., Mackay, J. B., Ward, R. X., & Arabas, S. (2023). New developments in PySDM and PySDM-examples v2:collisional breakup, immersion freezing, dry aerosol initialization, andadaptive time-stepping. *Journal of Open Source Software*, *8*(84), 4968. https://doi.org/10.21105/joss.04968